Mémoire

Auteur : De Kesel, Laure
Promoteur(s) : Cudell, Jean-René
Faculté : Faculté des Sciences
Diplôme : Master en sciences spatiales, à finalité approfondie
Année académique : 2023-2024
URI/URL : http://hdl.handle.net/2268.2/21209

Puzzle of neutrino oscillations

Laure De Kesel

Master thesis in Space Sciences
Research Focus

Faculty of Sciences

Department of Astrophysics, Geophysics
and Oceanography

Academic year 2023-2024

Acknowledgments

Here we are. This is a strange feeling; I am in a sort of mixed state between joy, sadness and fear to eventually have come this far on this journey. My last years of studies were quite difficult to handle due to an accumulation of personal issues as well as external events beyond my control. To be honest, I felt like these two past years would never end and that I would not be able to get through it. With the benefit of hindsight, I noticed this period of my life led me to a kind of «*a human-supernovae experience*»; I collapsed inside while everything was highly perturbed around me. And I could not recommend a more suitable life experience to get back to essentials and the importance of the small things. No matter what might have happened under different circumstances, now that the storm has passed I can attest the people we surround ourselves with have a huge impact.

I was lucky to be able to count on my parents' support in all circumstances. I will never be able to thank them enough for everything they have done for me. Words could not adequately express what I would tell them.

Then, among the variety of people I met during my first reckless years of studies, I met valuable persons who have continued to have a major impact on my life. I especially think of Somers, Lydia, Emilien, Jona, Antoine and Groulard. Each discussion and adventure with you was always helpful and entertaining. Thank you for being there, you are like a little sunshine to me.

The next indispensable one is my supervisor for this work, Prof. Jean - René Cudell. The first thing I should thank you for is your patience. But I mostly want to thank you for having supported me since the beginning and for your wise advice. I was so afraid to ask you for a project to work on, and it turned out to be the best positive surprise of my studies. You allowed me to work on a project I enjoyed and above all, you helped me regain my self-confidence. Similarly as neutrinos transport most of the energy away during a supernova event, working on them allowed me to let go of many fears and to discover many things −about myself and about neutrinos. I have rediscovered that life can be fascinating.

My work on this master thesis was a major step and I thus thank the members of the reading committee: Dr. Valérie Van Grootel, Dr. Michaël De Becker and Dr. Gregor Rauw to have kindly accepted to read it.

Finally, let's remind us that despite all we are going through at the moment, the most magnificent gift is to be surrounded by the right people. I had this chance. So again, I address my sincerest thanks to all of you.

Abstract

The 20^{th} century was a thriving era for many fields in sciences, including particle physics with the establishment of the Standard Model. When the Standard Model was first proposed, neutrinos were supposed to appear as three flavours corresponding to the lepton produced when the neutrino interacts and having no mass. However late 1960s, scientists were confronted to *the solar neutrino problem* and their conception of neutrinos had to change. The long journey up to the discovery of neutrino oscillations in solar and atmospheric neutrinos −which enables one flavour to change into another during its course over time− imposes those particles have a mass. Consequently neutrinos have been extensively studied on the one hand to determine their properties (*i.e.* to put constraints on their mass, to know how they interact with matter, know if they are their own antiparticle,...) and on the other hand to study their oscillations and constraint the allowed range of parameter values. There are six parameters: two squared mass differences, three angles and at least one phase. The formalism was well established and the two mass differences allowed correspond to the mass difference observed in solar neutrino oscillations and to the mass difference observed in atmospheric neutrino oscillations. By 2000, the situation was much clearer. However, some experiments reported unexpected parameter values, challenging our comprehension of neutrino oscillations. In total three types of anomalies are reported; the LSND, the Gallium and the reactor antineutrino anomaly. We will focus here on the first one, which was an anomaly initially reported by the *Liquid Scintillator Neutrino Detector* experiment in 1995 and was confirmed in 2009 by the MiniBooNE experiment. These new parameter values do not fit in the actual scheme of three neutrino mixing and may imply new physics.

In this work, we will start with an introduction to neutrino oscillations in chapter 1, where we will then present the formalism of three neutrino mixing as understood nowadays. In chapter 2 we will describe the MiniBooNE experiment and review its results. Next, in chapter 3, we will derive the deviation of the observed number of events compared to the expected one to understand better the importance of the anomaly. We will also derive the oscillation parameter values with this new set of data to see how these insert into the actual scheme. We will continue with a discussion about the currently most investigated solution; the existence of additional *sterile neutrinos* whose further investigation experiments are presented in chapter 4.

Table of contents

Chapter 1

Introduction

1.1 Neutrino and oscillation discovery

Our knowledge of neutrinos dates back to 1930 when scientists were intensively studying the energy spectrum of beta radiations. As they initially thought that beta particles were the only ones emitted during the radioactive decay of atoms, they must have had well-defined discrete energies. However, these displayed continuous energy and momentum spectra. A solution proposed by W. Pauli was the existence of an undetected particle to ensure the conservation of energy and momentum [1]. E. Fermi followed this idea and built the first pieces of the weak interaction theory in 1934 with those *neutrinos* −namely « the small neutral one »− having a zero charge, a spin $\frac{1}{2}$, a small mass (i.e. at most the mass of the electron) and interacting weakly as it was hard to detect directly [2]. Its existence was eventually proved experimentally in 1956 thanks to C. Cowan and F. Reines, who actually detected an electron antineutrino from nuclear fission in a reactor through inverse beta decay i.e. antineutrino-proton scattering $\overline{\nu}_e + p \rightarrow e^+ + n$ [3]. Nowadays, we know that neutrinos appear in three *flavours*; the muon neutrino was discovered in 1962 [4] and the tau neutrino in 2000 [5]. The neutrino flavour corresponds to that of the lepton produced when it interacts.

The weakly interacting property of those particles[1] is in part a real asset as it means they are a direct source of information about their environment. In 1962, J. N. Bahcall wanted to harness this property to obtain the first direct evidence of nuclear energy generation in stars by counting solar neutrinos we receive on Earth [7] [8]. The experiment J. N. Bahcall and R. Davis conceived for this purpose −referred to as the *Homestake experiment* [9]− started operation in 1967 in the Homestake Gold Mine (North America), 1478 metres underground. The apparatus inside the rock cavity consisted of a 6.1 m diameter and 14.6 m long horizontal tank filled at 95% with 615 metric tons of tetrachloroethylene (C_2Cl_4) and the remaining 5% was helium gas on top. The tank was itself flooded with water in the cavity. Neutrinos were detected through the inverse beta decay of chlorine nuclei: $\nu_e + {}^{37}Cl \rightarrow {}^{37}Ar + e^-$. The energy threshold of the detector was 0.814 MeV, implying it was sensitive to ${}^8B$, pep and hep neutrino production in the Sun. Fig. 1.1 shows energy spectra and fluxes of solar neutrino, that depend on the nuclear reactions these originate from as well as the sensitivity of the various solar neutrino

[1] Its cross section is extremely small: 1.1 10^{-38} cm^2 at 1 GeV for neutrinos and it is roughly the half for antineutrinos: 0.35 10^{-38} cm^2 [6].

experiments.

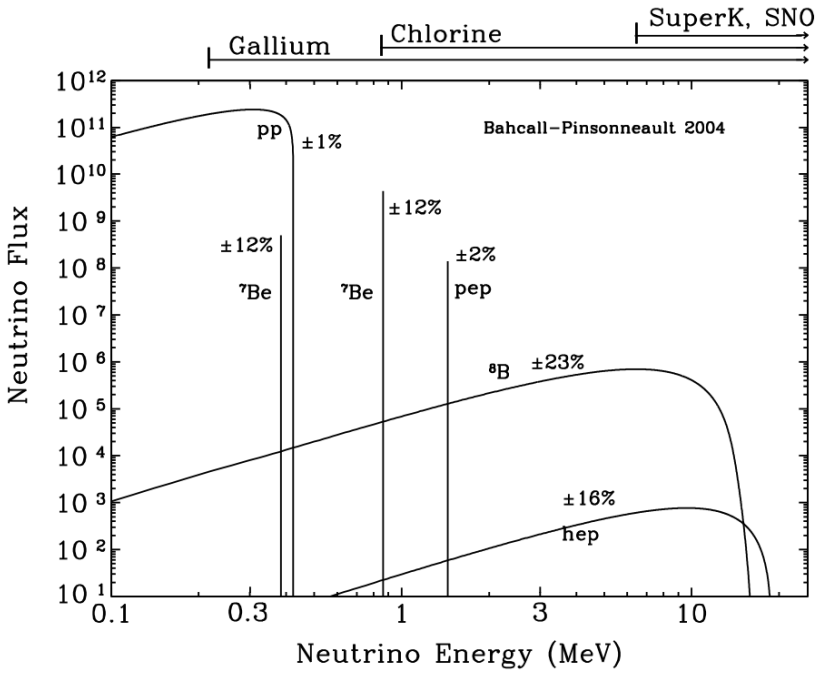

Figure 1.1: Predicted solar neutrino energy spectrum depending on the reaction in the Sun responsible for their production according to the 2004 standard solar model of Bahcall and Pinsonneault. Taken from [10]. The energy thresholds of different solar neutrino detection experiments are also noted. Fluxes are expressed in $\mathrm{cm}^{-2}\mathrm{s}^{-1}\mathrm{MeV}^{-1}$.

The underground location is necessary to minimise cosmic ray contamination by providing an average overburden for the detector of 4 200 ± 100 metres water equivalent. Cosmic rays are a high-energy massive flux of charged particles[2] that collides with atomic nuclei in the atmosphere and produce *particle showers* i.e. a particle decaying into others which can themselves be energetic enough to collide with nuclei and produce other particles and so on [11]. After a collision of the primary cosmic ray with molecules of the atmosphere, we are left with a fragmented nucleus, pions and some photons. A pion can decay in three different ways depending on its charge; π^0 decays into two photons and sometimes one photon converts into a pair of electron-positron, charged pions most generally decay as

$$\pi^+ \to \mu^+ + \nu_\mu \quad \text{followed by} \quad \mu^+ \to e^+ + \nu_e + \overline{\nu}_\mu \tag{1.1}$$

$$\pi^- \to \mu^- + \overline{\nu}_\mu \quad \text{followed by} \quad \mu^- \to e^- + \nu_\mu + \overline{\nu}_e \tag{1.2}$$

At some point, the particles are not energetic enough to continue this particle chain reaction and only elastic scattering happens. Plenty of energetic muons are produced which are very penetrating and can knock protons out of atomic nuclei below the earth's surface. If those enter the detector, they would turn chlorine into argon with the release of a neutron and thus mimic the entry of a solar neutrino. Nonetheless, rock walls present natural radioactivity and are a source of alpha particles and fast neutrons. Those neutrons can produce argon if they have a minimum energy of 1 MeV to initiate the following

[2]They are made of mostly protons, alpha particles, electrons and other nuclei of heavier elements.

reactions: $^{35}Cl + n \rightarrow p + {}^{35}S$, $^{37}Cl + p \rightarrow n + {}^{37}Ar$. Those are stopped thanks to the external water shielding. About alpha particles, these can also come from radioactivity within the tank due to the materials used. These are a source of contamination as their interaction in the detector can produce protons. Those three main sources of non-solar argon atoms produced in the detector[3] were carefully studied to determine their associated rate of production, which was subtracted from the overall computed argon production.

Argon atoms from solar neutrinos are collected through an extraction process. That consists of a purge of the liquid with helium gas. During this process, pumping systems mix the helium on top and tetrachloroethylene together in the detector and simultaneously sweep helium through an adsorber that adsorb argon out of helium. The trapped argon is then chemically purified and inserted into a proportional counter to determine the number of atoms recovered. Extractions are done every few weeks to prevent argon from decaying back (Ar $\tau_{1/2} = 35$ days). Their first results, published in 1968, revealed a much lower flux than predicted. The solar neutrino flux production rate is expressed in terms of *solar neutrino units* (SNU) where one SNU corresponds to one neutrino captured per second in a target containing 10^{36} atoms of isotope capturing neutrinos. The observed production rate was 3 SNU while the theoretically expected flux from their solar standard model (SSM) was 20 SNU [12]. Even with further adjustments and refinement of their solar model, a deficit of roughly two-thirds with respect to the predicted flux remained. In their latest results [9], which corresponds to the analysis of 1970 to 1995 data, they observed a production rate of 2.56 ± 0.16 (stat.) ± 0.16 (syst.) SNU while the theoretical prediction was $9.3^{+1.2}_{-1.4}$ SNU [13]. This marked the beginning of the *solar neutrino problem*.

Highly motivated to understand what was happening and to search for other possible anomalies in the spectrum, experiments with higher and lower sensitivity were built in the following decades. Firstly there was the *KamiokaNDE* experiment [14] −which stands for Kamioka Nucleon Decay Experiment[4]− that operated from 1987 to 1996. It was located in the Kamioka mine (Japanese Alps), 1000 m underground at 2700 m water equivalent. It consisted of a cylindrical steel tank of 16 m high and 15.5 m in diameter, filled with 3000 tons of pure water. The inner surface was covered at 20% with 948 photomultiplier tubes (PMTs). This is a *water Cherenkov detector*, detection of particles is made through Cherenkov radiation; a cone of blue light. It happens when high-energy charged particles travel in a dielectric medium at a velocity faster than the speed of light in that medium. The successive electromagnetic wave fronts accumulate and form a conic shape shock front of light whose angle is related to the particle's velocity, hence its energy. Thus each particle has an associated particular pattern. The PMTs record the light quantity detected during an event as well as the timing of detection and enable scientists to see the Cherenkov radiation of products of interaction and consequently reconstruct the interaction kinematics. Also called *real-time detectors* these enable individual event study and are independent of the SSM used. To reject background events (mostly muons produced by cosmic rays) there are two veto counters; one at the top and one at the bottom. These PTMs are located behind a steel plate 25 cm thick to identify cosmic ray

[3]Given that this discussion can be extended for the solar neutrino experiments that follows, it will not be presented anymore.

[4]The detector was originally built in 1983 to search for proton decay signals but detected nothing apart a background noise anomaly coming from neutrinos. The detector was consequently upgraded in 1985 to observe solar neutrinos and started operation for this purpose in 1987. Furthermore, it measured events of SN1987A.

muons that pass through the detector. The cavity was flooded with water to provide with side shielding from cosmic ray muons and from photons and neutrons due to rock wall radioactivity. With an energy threshold of 7 MeV, this experiment was mainly sensitive to ^8B solar neutrinos. In Fig. 1.1, the Kamiokande experiment would be located a little bit after *SuperK, SNO*. The neutrino detection was made from recoil electrons of water after elastic collision from neutrino interaction. Due to conservation of momentum and studies of scattering kinematics, we know the recoil electron goes in roughly the direction of the initial neutrino trajectory and the Kamiokande experiment was the first to demonstrate that observed neutrinos were indeed coming from the Sun. The experiment also reported observations of one-half of the predicted flux. Their latest results [15], which combined data from 1987 to 1995, reported 390^{+35}_{-33} solar neutrino events while 785 events were expected. This way this second experiment also provided evidence for neutrino deficit in the high- energy part of the solar neutrino spectrum.

Secondly, there were gallium experiments to measure the low-energy neutrinos led by the *SAGE* and *GALLEX* collaborations. With an energy threshold of 233 keV, these are mainly sensitive to ^7Be and pp solar neutrinos. Both experiments used liquid gallium whose neutrino detection is by means of inverse beta decay: $^{71}Ga + \nu_e \rightarrow e^- + \ ^{71}Ge$. As the Homestake experiment, these are also radio-chemical detectors and the principle of working is similar. The main sources of contamination are also protons and fast neutrons coming from cosmic ray muons and external and internal radiations. A major difference with the first experiment is that pp neutrinos were proven to be proportional to solar luminosity and thus the theoretically expected production rate has the advantage of being insensitive to variations in the SSM used [16].

The SAGE experiment [17] −which stands for Soviet-American Gallium Experiment− started operation in 1990 and consisted of a tank filled with roughly 50 tons of liquid metal gallium. It was located 2100 m underground in the northern Caucasus mountains (Russia), at 4700 m of water equivalent. Instead of external water shielding, the detector had a lining of 60cm low-radioactivity concrete with an outer 6 mm steel shell. The extraction process was done by selective oxidation of germanium by an aqueous solution. This solution underwent some manipulations to eventually allow scientists to synthesize germane, GeH_4 gas, which is then purified to isolate germanium. The last step consists of putting it into a proportional counter to know the number of atoms recovered. Extraction processes are done every 6 weeks (Ge $\tau_{1/2} = 11.43$ days). Results of the collaboration observations for the period of 1990 to 1997 present a capture rate of slightly more than one-half of the prediction; $67.2^{+7.2}_{-7.0}(\text{stat.})^{+3.5}_{-3.0}(\text{syst.})$ SNU while the theoretical models amounted to 129^{+8}_{-6} SNU [18]. Next, the GALLEX experiment [19] −which stands for GALLium EXperiment− started operation in 1991 and was located inside the Gran Sasso mountain (Italy) at 3200 metres of water equivalent. It constituted of a tank filled with 100 tons of a gallium chloride solution $(GaCl_3)$[5] and the extraction process was done here with a nitrogen purge of the liquid. The collaboration also reported an observed capture rate of slightly more than one-half; during its period of operation from 1991 to 1997 the observed flux was 76.4 ± 8 [19] while the theoretically expected flux is 129 SNU[6]. Consequently, gallium experiments show evidence of neutrino deficit at low energies too.

[5] « This chemical form was chosen to facilitate the extraction of the product, ^{71}Ge, as volatile germanium chloride $(GeCl_4)$ » [19]

[6] For the next years, from 1998 to 2003, the experiment pursued under the name *GNO* −Gallium Neutrino Observatory− which also reported roughly one-half of the predicted production rate after 5 years of operation [20].

In 1996, the Kamiokande experiment was dismantled and an upgraded version of it −the *Super Kamiokande* (SK) experiment− was built [14]. Still in the Kamioka mine, the apparatus now consists of a cylindrical tank 42 m high and 39 m in diameter containing a stainless superstructure that supports inward and outward-facing PMTs. The inner tank surface is photosensitive at 40% with 11200 PMTs and this structure delimits an inner tank of 36.2 m high and 33.8 m in diameter which is about 20 times larger than the available volume for particle detection in the Kamiokande experiment. Both volumes are filled with ultra-pure water. The outer volume again serves as shielding and as a veto counter. The structure is attached to an outer concrete layer as additional shielding. The principle of detection is obviously the same but the experiment is more sensitive. It can reject background down to lower energies which enables the energy threshold to be reduced down to 5.5 MeV. Their first results appeared in 2001 [21] and concluded in a measured flux of 2.32 ± 0.03 (stat.) $^{+0.08}_{-0.07}$ (syst.) 10^6 cm^{-2}s^{-1} which is one-half of that predicted as well. Nearly at the same time, the *Sudbury Neutrino Observatory* (SNO) also started to observe ^8B solar neutrinos aftermath the proposition of H. H. Chen [22] to solve the solar neutrino problem. Their first results published in 2001, presenting their results since the start of operation in 1999, eventually gave the solution to that puzzle [23]. This detector was located in Creighton mine near Sudbury (Canada) at 6010 m of water equivalent, 2100 m underground. The apparatus inside the cavity consisted of a spherical acrylic vessel of 12 m in diameter filled with 1 000 metric tons of heavy water (D_2O), surrounded by ultra pure water. The acrylic vessel was transparent in the visible portion of the electromagnetic spectrum, and about 9 500 PMTs stood on a stainless steel structure of 17.8 m in diameter. The external water again served as radiation shielding and particle identification with some PMTs located outside to detect cosmic ray muons that enter the detector. The energy threshold was 5 MeV. The presence of deuterium enables to distinct between reactions sensitive to electron neutrino only from those sensitive to all flavours equally likely. The former happens when a neutrino converts a neutron of a deuterium into a proton:

$$\nu_e + n \rightarrow p + e^-$$

Given this reaction is mediated by one of the charged boson of the electroweak interaction, it is referred to as *charged current* (CC) reaction. As solar neutrinos have energies smaller than the mass of muon and tau leptons, only electrons can be produced and thus only ν_e participate in this reaction. Electrons carry away almost all of neutrino's energy (between 5 to 15 MeV) and are easily detectable by the PMTs (whose kinetic energy threshold was 6.75 MeV) while the proton is usually not. Two additional reactions can happen with any neutrino flavour; electron elastic scatterings of atomic electrons and deuterium nucleus breaking into its constituents:

$$\nu + D \rightarrow p + n$$

Those two latter reactions are mediated by the neutral boson Z of the electroweak interaction and are thus referred to as *neutral currents* (NC) for this reason[7]. In their first publication [24] the collaboration reported data concerning the CC and elastic scattering rates and the associated fluxes; the ES flux was 2.39 ± 0.34 (stat.) $^{+0.16}_{-0.14}$(syst.) 10^6 cm^{-2}s^{-1} which was consistent with the previous result of SK. However, the CC flux was significantly smaller; $\nu_e = 1.75 \pm 0.07$ (stat.) $^{+0.12}_{-0.11}$ (syst.) $\pm$ 0.05 (theory) 10^6 cm^{-2}s^{-1}. There

[7]By using the NC abbreviation we will refer here to the second reaction only.

is a 3.3σ difference compared with the value retrieved of SK collaboration[8] and the probability that a downward fluctuation of the SK result would have produced the observed result at SNO is 0.04%, which provides strong evidence of non-electronic flavour component in the solar neutrino flux. Since only ν_e are produced in the Sun and that other flavours of neutrinos may reach us, neutrinos seem to oscillate into another flavour during propagation. This phenomenon was confirmed one year later with the publication of the SNO NC flux. This reaction was identified by further neutron capture which has a specific signature; either it is captured by a deuterium nuclei and a gamma ray with 6.25 MeV is emitted, or it is captured by water and a gamma ray of roughly 2.2 MeV is emitted. The cross-section of the neutron is much larger in water than in deuterium, however the 2.2 MeV gamma ray emitted in this case is not detectable by the PMTs. It can be if it further collides with an electron (in the case of Compton scattering) and the accelerated electron is detected through Cherenkov radiation. To enhance the neutron capture, the collaboration added 2 tonnes of salt ($NaCl$) uniformly distributed in the heavy water during the second phase of the experiment, from 2001 to 2003 [25].The presence of salt increases the neutron capture efficiency in heavy water as the cross-section on ^{35}Cl is much larger than that in water[9] and photons produced have a higher energy of 8.6 MeV which is more easily detected by the PMTs. This way the detection efficiency was multiplied by a factor of three. The updated flux values (expressed in 10^6 cm^{-2}s^{-1}) of the SNO collaboration are

$$\begin{aligned}
\phi_{CC} &= 1.70 \pm 0.07(\text{stat.})^{+0.09}_{-0.10}(\text{syst.}),\\
\phi_{ES} &= 2.13^{+0.29}_{-0.28}(\text{stat.})^{+0.15}_{-0.08}(\text{syst.}),\\
\phi_{NC} &= 4.90 \pm 0.24(\text{stat.})^{+0.29}_{-0.27}(\text{syst.}),\\
\phi_{Total} &= 5.21 \pm 0.27(\text{stat.}) \pm 0.38(\text{syst.}).
\end{aligned}$$

where the total flux is in concordance with the SSM prediction of 5.79±1.33 10^6 cm^{-2}s^{-1} of J. N. Bahcall and M. H. Pinsonneault in 2004 [26], whereas the ratio ϕ_{CC}/ϕ_{NC} is of one-third. Consequently, it confirmed that only one-third of neutrinos that reach us are of electronic flavour and that two-thirds oscillated into another flavour. The SNO experiment was very necessary to prove the oscillation hypothesis given that water Cherenkov detectors are in fact sensitive to all flavours but with an enhanced sensitivity for ν_e.

During solar neutrino hunting, the Kamiokande experiment pointed out pieces of evidence of oscillations in atmospheric neutrinos too. For 1986 upgrades to better differentiate candidate signals from background atmospheric neutrino interactions, scientists focused on that background and got on establishing theoretical simulation of atmospheric neutrinos. As seen on Eq.(1.1) and Eq.(1.2), $2(\nu_\mu + \overline{\nu}_\mu)$ and $1(\nu_e + \overline{\nu}_e)$ are produced for every charged pion decay. To be able to conclude whether a deficit or not independent of the details of neutrino production flux, scientists looked at their ratio[10] which is supposed to be about 2. The absolute flux predicted this way was shown to have a precision of approximately 20% [27]. The collaboration's first results about atmospheric neutrinos in

[8]Due to the large errors on their ES flux, the difference with the CC flux is not big and they thus compared with the more precise SK collaboration ES flux.

[9]$\sigma_{(n,^2H)} = 0.0005$ mb while $\sigma_{(n,^{35}Cl)} = 44$ mb.

[10]Many calculations were done to confirm the ratio value, see for example [27] and references therein. The uncertainty of this prediction is less than 5%.

1988 [28] reported a deficit of 40% of muon neutrinos in the sub-GeV energy range compared to the simulation; 85 ± 9.2 μ-like events were observed compared to 144.0 predicted by the MC simulation. The number of electron neutrinos was in good agreement; 93 ± 9.6 e-like events were detected compared to 88.5 predicted. The collaboration checked that the deficit could not be due as the result of systematic detector effects or uncertainties in the calculations. Moreover, to track evidence of oscillation, the flux was separated in its upward and downward direction by means of dependence of zenith angle Θ −the angle of the event direction relative to the vertical axis of the detector−. The upward component consists of $\cos\Theta$ values ranging from -1 to -0.2 and the downward component consists of $\cos\Theta$ values ranging from 0.2 to 1. Indeed, the cosmic ray flux is isotropic and one expects an up-down symmetric flux[11]. However if one assumes oscillations, neutrinos typically oscillate over a length of 100 km or longer[12] and vertically downward-going neutrinos that travel the atmosphere thickness do not have time to oscillate while upward-going neutrinos may have enough time as those travel nearly the Earth's diameter distance. The collaboration confirmed a significant zenith angle-dependent deficit of μ-like events; the ratio Up/Down was $0.58^{+0.13}_{-0.11}$. It represents 2.9σ but with the restriction on multi-GeV events, the volume was not large enough to limit statistical significance to the data and measurements kept on with the SK detector. To lower uncertainties, they compared the ratio $\mathcal{R} = \frac{(\mu\text{-like}/e\text{-like})_{Data}}{(\mu\text{-like}/e\text{-like})_{MC}}$. Their first results [29] reported small values of $\mathcal{R}$ both above and below 1 GeV; $\mathcal{R} = 0.63\pm$ 0.03 (stat.) ± 0.05 (syst.) for sub-GeV data and $\mathcal{R} = 0.65 \pm 0.05$ (stat.) ± 0.08 (syst.) for multi-GeV data. They also observed a zenith angle-dependent deficit of ν_μ with an Up/Down ratio of $= 0.54^{+0.06}_{-0.05}$ pointing to an upward deficit above 1 GeV compared to simulation expectations. The probability for statistical fluctuations as a way to explain those $\mathcal{R}$ values is less than 0.001% for sub-GeV and less than 1% for multi-GeV. In that paper, they presented an analysis where values are interpreted as oscillations of $\nu_\mu \leftrightarrow \nu_\tau$ at 90% confidence level in which the Kamiokande and SK data are consistent and thus the atmospheric neutrino anomaly was concluded to be due to neutrino oscillations in 1998. Since then, the SK collaboration reported many results with improved measurements and increasing precision.

In addition to solar detection experiments, there were experiments with man-made neutrino sources at reactors and accelerators. The first reactor experiment was led with *KamLAND* [30] −which stands for Kamioka Liquid scintillator Anti-Neutrino Detector− in 2002. It consisted of a liquid scintillator detector located at the old Kamiokande cavity where many nuclear reactors exist nearby. Those furnish a source of $\overline{\nu}_e$ which travels about 180 km before reaching the detector. Its results were consistent with solar experiments and showed that fewer $\overline{\nu}_e$ were observed than expected. Furthermore the ratio of observed over expected events clearly showed an oscillatory pattern. On the other hand the first accelerator (of long-baseline) was *T2K* [31] that operated from 1999 to 2004. It was designed to verify atmospheric oscillations with the use of a neutrino beam produced at KEK and observed 250 km further at SK. It observed a deficit of ν_μ whose probability to be explained by statistical fluctuations with no neutrino oscillations is 0.0015%. It corresponds to 4.3σ which also confirmed the oscillation hypothesis. Since then, numerous other reactors experiments (like *Daya Bay [32], Double Chooz, RHF* and *TEXO*) and accelerators experiments (like *MINOS, ICARUS, NOνA* and *OPERA*)

[11] Due to geomagnetic field effect it is not totally exact for sub-GeV neutrinos but it is expected for multi-GeV neutrinos. The collaboration thus studied multi-GeV events only.

[12] See Fig. 1.2

studied oscillations and have constrained many of the parameters with increasing levels of precision. A three-neutrino mixing scheme has been established and its basics are presented in the next section.

1.2 Basic formalism of neutrino oscillation

This section is based upon references [1], [11] and [33].

After the neutrino discovery, experiments in hopes of measuring its mass found that it would be so tiny that it may be zero. The Standard Model was then established with neutrinos having a zero mass. However, the oscillation phenomena imply that neutrinos have a mass. Their masses are not yet known because they are so tiny that no experience has succeeded in measuring them and present measurements bound it to be < 2 eV. The standard model describes the neutrino as a unitary quantum mechanical combination of three *neutrino mass states* ν_1, ν_2 and ν_3, having small masses, respectively m_1, m_2 and m_3. The difference in mass makes these travel at slightly different velocities which produces a phase shift that changes the combination of the mass states during propagation and affects in turn the flavour of the neutrino. The flavour eigenstates $|\nu_\alpha\rangle$, (where α refers to electron, muon or tau) are a linear combination of mass eigenstates $|\nu_i\rangle$ (where i refers to 1, 2 or 3). This way, the mixing is expressed via a unitary mixing matrix U:

$$|\nu_\alpha\rangle = \sum_{k=1}^{3} U_{\alpha k}|\nu_k\rangle \tag{1.3}$$

where the mixing matrix is the Pontecorvo–Maki–Nakagawa–Sakata (PMNS) matrix which can be parameterized as

$$\begin{aligned} U_{\alpha i} &= \begin{pmatrix} U_{e1} & U_{e2} & U_{e3} \\ U_{\mu 1} & U_{\mu 2} & U_{\mu 3} \\ U_{\tau 1} & U_{\tau 2} & U_{\tau 3} \end{pmatrix} \\ &= \begin{pmatrix} 1 & 0 & 0 \\ 0 & \cos(\theta_{23}) & \sin(\theta_{23}) \\ 0 & -\sin(\theta_{23}) & \cos(\theta_{23}) \end{pmatrix} \begin{pmatrix} \cos(\theta_{13}) & 0 & \sin(\theta_{13})e^{-i\delta} \\ 0 & 1 & 0 \\ -\sin(\theta_{13})e^{i\delta} & 0 & \cos(\theta_{13}) \end{pmatrix} \begin{pmatrix} \cos(\theta_{12}) & \sin(\theta_{12}) & 0 \\ -\sin(\theta_{12}) & \cos(\theta_{12}) & 0 \\ 0 & 0 & 1 \end{pmatrix}. \end{aligned} \tag{1.4}$$

where θ_{ij} are the three mixing angles and δ is a phase. That phase corresponds to the CP violation phase; if it is different from 0 or π it would imply neutrinos and antineutrinos do not behave the same. In general parametrisation it is allowed to take any value.

Let us note the PMNS matrix can be further multiplied by two factor phases such as

$$\begin{pmatrix} e^{i\eta_1} & 0 & 0 \\ 0 & e^{i\eta_2} & 0 \\ 0 & 0 & 1 \end{pmatrix}$$

if we consider *Majorana neutrinos*, that is to say neutrinos that would be their own antiparticles. This idea was proposed by E. Majorana in 1937 and the most investigated search to prove it is via the detection of two single β-decays occurring simultaneously where no neutrinos are observed in the final state as these would annihilate each other. We thus speak about a *neutrinoless double β-decay*. This reaction has been actively searched for, for example by experiments *KamLAND-Zen* [34], *GERDA* [35] and *EXO-200* [36],

but has not been detected yet. Generally one considers *Dirac neutrinos* −*i.e.* neutrinos that are distinct particles from antineutrinos− since there is yet no evidence in favor of Majorana neutrino hypothesis. Furthermore the principle of oscillation is not impacted by this description of neutrinos[13].

Consequently, a flavour state evolves over time as

$$|\nu_\alpha(t)\rangle = \sum_{k=1}^{3} U_{\alpha k} \, |\nu_k(t)\rangle$$

and the probability for this neutrino to turn into another flavour β after a traveled distance L is defined as[14]

$$P(\nu_\alpha \to \nu_\beta) \equiv P_{\alpha\beta} = |\langle \nu_\beta | \nu_\alpha(t) \rangle|^2 = \left| \sum_{k=1}^{3} \sum_{j=1}^{3} U_{\alpha k} U^*_{\beta j} \langle \nu_j \, | \nu_k(t) \rangle \right|^2 . \tag{1.5}$$

We use natural units so that $c = \hbar = 1$. We assume a plane-wave solution which is of the form

$$|\nu_k(t)\rangle = e^{-iE_k t} \, |\nu_k(0)\rangle$$

where E_k is the energy of the mass eigenstate k and p is the neutrino momentum. Neutrinos travel nearly at the speed of light and in the relativistic limit (*i.e.* $p >> m_k$) we can approximate the energy as

$$E_k = \sqrt{p_k^2 + m_k^2} \simeq p_k + \frac{m_k^2}{2p_k} \approx p + \frac{m_k^2}{2E}$$

and $t \approx L$ thus

$$|\nu_k(t)\rangle = e^{-i\left(p + \frac{m_k^2}{2E}\right)L} \, |\nu_k\rangle \tag{1.6}$$

and finally

$$|\nu_\alpha(t)\rangle = \sum_{k=1}^{3} U_{\alpha k} e^{-i\left(p + \frac{m_k^2}{2E}\right)L} \, |\nu_k(t)\rangle \, . \tag{1.7}$$

Given eigenstates are orthonormal $\langle \nu_j | \nu_k \rangle = \delta_{jk}$ and by denoting $m_k^2 - m_j^2 = \Delta m_{kj}^2$

[13] The interested reader can find more information on this subject in the references [37] and [38].

[14] As a convention throughout this work: the * index indicates the complex conjugate matrix.

the transition probability can be rewritten

$$\begin{aligned} P_{\alpha\beta} &= \left| \sum_{k=1}^{3} U_{\alpha k} U_{\beta k}^{*} e^{-i\left(p+\frac{m_k^2}{2E}L\right)} \right|^2 \\ &= \left(\sum_{k=1}^{3} U_{\alpha k} U_{\beta k}^{*} e^{-i\frac{m_k^2}{2E}L} \right) \left(\sum_{j=1}^{3} U_{\alpha j} U_{\beta j}^{*} e^{-i\frac{m_j^2}{2E}L} \right)^{*} \\ &= \sum_{k=1}^{3}\sum_{j=1}^{3} U_{\alpha k} U_{\beta k}^{*} U_{\alpha j}^{*} U_{\beta j} e^{-i\left(\frac{\Delta m_{kj}^2 L}{2E}\right)} \\ &= \sum_{k=1}^{3} U_{\alpha k} U_{\beta k}^{*} U_{\alpha k}^{*} U_{\beta k} + \sum_{k\neq j}^{3} U_{\alpha k} U_{\beta k}^{*} U_{\alpha j}^{*} U_{\beta j} e^{-i\left(\frac{\Delta m_{kj}^2 L}{2E}\right)} \end{aligned}$$

We then expand the exponential as $e^{-iz} = \cos z - i \sin z = 1 - 2\sin^2 \frac{z}{2} - i \sin z$, and we obtain

$$\begin{aligned} P_{\alpha\beta} = \underbrace{\sum_{k=1}^{3} U_{\alpha k} U_{\beta k}^{*} U_{\alpha k}^{*} U_{\beta k} + \sum_{k\neq j}^{3} U_{\alpha k} U_{\beta k}^{*} U_{\alpha j}^{*} U_{\beta j}}_{\text{A}} - 2 \underbrace{\sum_{k\neq j}^{3} U_{\alpha k} U_{\beta k}^{*} U_{\alpha j}^{*} U_{\beta j} \sin^2\left(\frac{\Delta m_{kj}^2 L}{4E}\right)}_{\text{B}} \\ - i \underbrace{\sum_{k\neq j}^{3} U_{\alpha k} U_{\beta k}^{*} U_{\alpha j}^{*} U_{\beta j} \sin\left(\frac{\Delta m_{kj}^2 L}{2E}\right)}_{\text{C}} \end{aligned} \quad (1.8)$$

The first two terms, term A, can be rewritten as

$$\begin{aligned} A &= \sum_{k=1}^{3}\sum_{j=1}^{3} U_{\alpha k} U_{\beta k}^{*} U_{\alpha j}^{*} U_{\beta j} \\ &= \sum_{k=1}^{3} |U_{\alpha k} U_{\beta k}^{*}|^2 = \delta_{\alpha\beta} \end{aligned}$$

due to the unitary property of U. Then, to rewrite the third term B we will exploit the fact that the change of Δm^2 sign in the $\sin^2$ function does not require a change of sign as

it is an even function. Next we redefine the indices of the second sum. Thus,

$$\begin{aligned}
B &= \sum_{k<j}^{3} U_{\alpha k}U^*_{\beta k}U^*_{\alpha j}U_{\beta j}\sin^2\left(\frac{\Delta m^2_{jk}L}{4E}\right) + \sum_{k>j}^{3} U_{\alpha k}U^*_{\beta k}U^*_{\alpha j}U_{\beta j}\sin^2\left(\frac{\Delta m^2_{kj}L}{4E}\right) \\
&= \sum_{k<j}^{3} U_{\alpha k}U^*_{\beta k}U^*_{\alpha j}U_{\beta j}\sin^2\left(\frac{\Delta m^2_{jk}L}{4E}\right) + \sum_{j>k}^{3} U_{\alpha j}U^*_{\beta j}U^*_{\alpha k}U_{\beta k}\sin^2\left(\frac{\Delta m^2_{kj}L}{4E}\right) \\
&= \sum_{k<j}^{3} (U_{\alpha k}U^*_{\beta k}U^*_{\alpha j}U_{\beta j} + U_{\alpha j}U^*_{\beta j}U^*_{\alpha k}U_{\beta k})\sin^2\left(\frac{\Delta m^2_{jk}L}{4E}\right) \\
&= \sum_{k<j}^{3} (U_{\alpha k}U^*_{\beta k}U^*_{\alpha j}U_{\beta j} + U^*_{\alpha k}U_{\beta k}U_{\alpha j}U^*_{\beta j})\sin^2\left(\frac{\Delta m^2_{jk}L}{4E}\right) \\
&= \sum_{k<j}^{3} (U_{\alpha k}U^*_{\beta k}U^*_{\alpha j}U_{\beta j} + (U_{\alpha k}U^*_{\beta k}U^*_{\alpha j}U_{\beta j})^*)\sin^2\left(\frac{\Delta m^2_{jk}L}{4E}\right) \\
&= 2\sum_{k<j}^{3} \mathcal{R}e[U_{\alpha k}U^*_{\beta k}U^*_{\alpha j}U_{\beta j}]\sin^2\left(\frac{\Delta m^2_{jk}L}{4E}\right).
\end{aligned}$$

We proceed in the same fashion for the last term C but this time the change of Δm^2 will need a change of sign of the sinus function.

$$\begin{aligned}
C &= -\sum_{k<j}^{3} U_{\alpha k}U^*_{\beta k}U^*_{\alpha j}U_{\beta j}\sin\left(\frac{\Delta m^2_{jk}L}{2E}\right) + \sum_{k>j}^{3} U_{\alpha k}U^*_{\beta k}U^*_{\alpha j}U_{\beta j}\sin\left(\frac{\Delta m^2_{kj}L}{2E}\right) \\
&= -\sum_{k<j}^{3} U_{\alpha k}U^*_{\beta k}U^*_{\alpha j}U_{\beta j}\sin\left(\frac{\Delta m^2_{jk}L}{2E}\right) + \sum_{j>k}^{3} U_{\alpha j}U^*_{\beta j}U^*_{\alpha k}U_{\beta k}\sin\left(\frac{\Delta m^2_{jk}L}{2E}\right) \\
&= \sum_{k<j}^{3} (U^*_{\alpha k}U_{\beta k}U_{\alpha j}U^*_{\beta j} - U_{\alpha k}U^*_{\beta k}U^*_{\alpha j}U_{\beta j})\sin\left(\frac{\Delta m^2_{jk}L}{2E}\right) \\
&= \sum_{k<j}^{3} ((U_{\alpha k}U^*_{\beta k}U^*_{\alpha j}U_{\beta j})^* - U_{\alpha k}U^*_{\beta k}U^*_{\alpha j}U_{\beta j})\sin\left(\frac{\Delta m^2_{jk}L}{2E}\right) \\
&= 2i\sum_{k<j}^{3} \mathcal{I}m[U_{\alpha k}U^*_{\beta k}U^*_{\alpha j}U_{\beta j}]\sin\left(\frac{\Delta m^2_{jk}L}{2E}\right)
\end{aligned}$$

If we put it all together, Eq.(1.8) becomes

$$\begin{aligned}
P_{\alpha\beta} = \delta_{\alpha\beta} - 4\sum_{k=1<j}^{3} \mathcal{R}e[U_{\alpha k}U^*_{\beta k}U^*_{\alpha j}U_{\beta j}]\sin^2\left(\frac{\Delta m^2_{jk}L}{4E}\right) \\
+ 2\sum_{k=1<j}^{3} \mathcal{I}m[U_{\alpha k}U^*_{\beta k}U^*_{\alpha j}U_{\beta j}]\sin\left(\frac{\Delta m^2_{jk}L}{2E}\right). \quad (1.9)
\end{aligned}$$

In its most common form the probability is rewritten with a dimensionless sinus argument[15] such that

[15]It is done by introducing the appropriate number of $\hbar$ and c constants that were washed out by the use of natural units:

$$\frac{\Delta m^2_{jk}L}{4E} = \frac{\Delta m^2_{jk}c^4}{4\hbar c}\frac{L}{E}.$$

We then replace the product $\hbar$c by its value ($\hbar$ = 1.0546 10^{-34} J.s = 6.5821 10^{-16} eV.s and c = 299792458 m/s) and multiply by 10^6 to account for the fact E is expressed in MeV whereas $\Delta m^2_{jk}c^4$ will be expressed in eV^2. We go back to natural units and the result further simplifies as in Eq.(1.10).

$$P_{\alpha\beta} = \delta_{\alpha\beta} - 4 \sum_{k=1<j}^{3} \mathcal{R}e[U_{\alpha k} U^*_{\beta k} U^*_{\alpha j} U_{\beta j}] \sin^2 \left(1.267 \Delta m^2_{jk} \frac{L}{E}\right) + 2 \sum_{k=1<j}^{3} \mathcal{I}m[U_{\alpha k} U^*_{\beta k} U^*_{\alpha j} U_{\beta j}] \sin 2 \left(1.267 \Delta m^2_{jk} \frac{L}{E}\right) \quad (1.10)$$

with the three squared mass differences Δm^2_{jk} expressed in eV^2, the length of oscillation L expressed in m and the energy of incident neutrinos E expressed in MeV. The two latter parameters are fixed by the experimental setup up and there remain **six free parameters**: three angles, two squared mass differences and one phase.

An oscillatory length ensues from Eq.(1.10):

$$\sin^2 \left(1.267 \Delta m^2_{jk} \frac{L}{E}\right) = \sin^2 \left(\pi \frac{L}{L^{osci}_0}\right)$$

where

$$L^{osci}_0 = 2.48 \frac{E}{|\Delta m^2_{jk}|} \quad (1.11)$$

is the length over which one full oscillation cycle happens in vacuum.

Consequently we see that if mass eigenstates had the same mass, the probability would be reduced to $P_{\alpha\beta} = \delta_{\alpha\beta}$ and neutrinos would keep their initial flavour during propagation. This last relation also shows that the squared mass difference influences directly the oscillation length. The baseline length and incident neutrino energy of experiments are fixed so that the experiment is most sensitive in the chosen energy range at which oscillations happen. The three possible cases are illustrated in Fig.1.2 which shows the neutrino survival probability as a function of length. This graph was generated using a two-neutrino approximation whose computation is detailed in Annex A. If the ratio L/E is much smaller than $\frac{2.48}{\Delta m^2_{jk}}$, the experiment is too close and there is no time for oscillation to happen. This situation corresponds to the (a) part of the graph. Contrarily, at a very large value of the ratio many oscillations have time to occur as seen in the (c) part of the graph. Thus the experiment cannot resolve the oscillation pattern but will rather measure an average transition probability $\sim \frac{\sin^2 2\theta}{2}$. Thus the experiment ratio has to be on the order or greater than $\frac{2.48}{\Delta m^2_{jk}}$ to detect an oscillation signal and the (b) region is the one with the most sensitivity. It happens when $L/E \approx \frac{1}{\Delta m^2_{jk}}$.

It turned out that solar and reactor antineutrino experiments results agreed on ν_e disappearance at $\Delta m^2 \sim 7\ 10^{-5}\ \text{eV}^2$ and results of atmospheric neutrinos and long-baseline accelerators agreed on ν_μ disappearance at $\Delta m^2 \sim 2\ 10^{-3}\ \text{eV}^2$. As we have two mass squared differences this means we have two possible lengths of oscillation. If we plot the oscillation probability now considering the case of three neutrinos, we can see the two distinct oscillation lengths generated by those two mass squared differences. This is done in Fig. 1.3 where an initial ν_e of 1 GeV is considered. At 1 GeV the shorter L^{osci}_0 generated by the atmospheric mass squared difference is about 992 km while the longer L^{osci}_0 generated by the solar mass squared difference is about 33460 km.

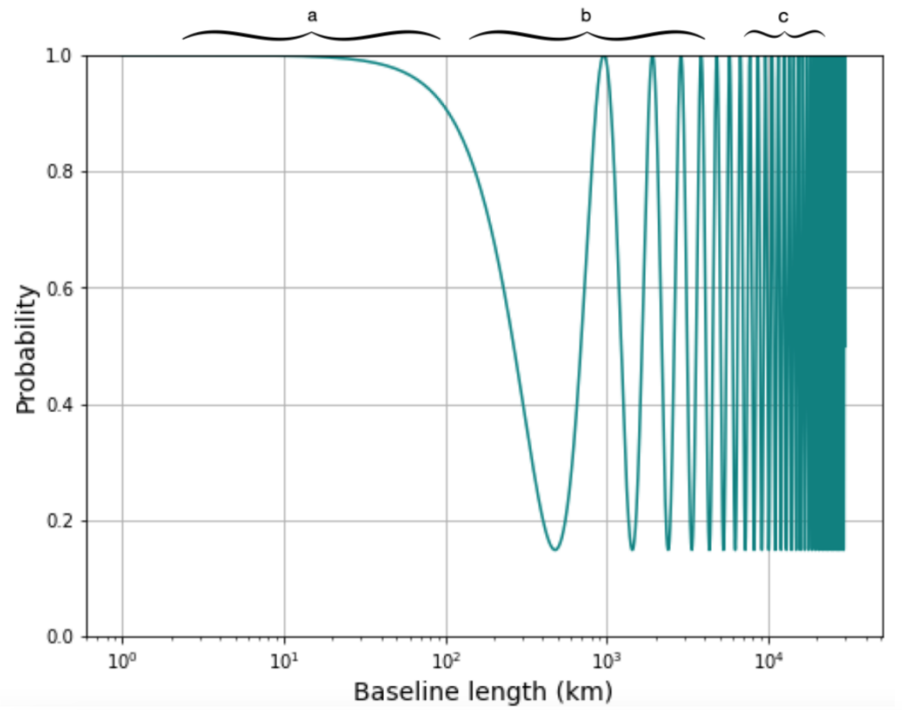

Figure 1.2: Logarithmic graph of the oscillation probability of a neutrino to keep its initial flavour as it propagates in vacuum. The three regions corresponds to places where the ratio L/E is much smaller (a), on the order of (b) and much larger (c) than $\frac{2.48}{\Delta m^2_{jk}}$. The graph was generated assuming a two-neutrino approximation of 1 GeV energy. A similar graph can be found in [33].

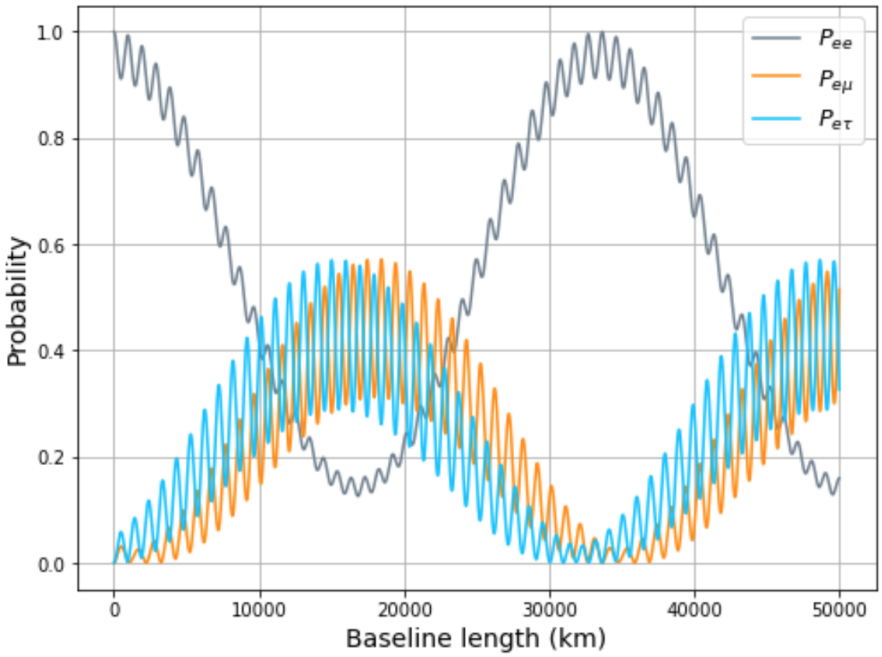

Figure 1.3: Plot showing the oscillation length due to the solar and atmospheric mass squared differences. The graph was generated considering an initial ν_e of 1 GeV.

Furthermore, even if we do not know neutrino masses yet we however know that m_1 and m_2 are really close so Δm^2_{21} corresponds to the smallest mass difference. What is still unknown is which one of m_1 or m_3 is the lightest mass which constitutes the *mass hierarchy problem*. The normal ordering (NO) supposes the ν_1 mass state as the lightest and contrarily the inverted ordering (IO) supposes the ν_3 mass state as the lightest. The values of the six needed parameters as derived from the various experiments are given in Table 1.1.

	Normal ordering	**Inverted ordering**
Δm^2_{21} $(10^{-5}$ eV$^2)$	$7.41^{+0.21}_{-0.20}$	$7.41^{+0.21}_{-0.20}$
Δm^2_{32} $(10^{-3}$ eV$^2)$	$2.505^{+0.024}_{-0.026}$	$-2.487^{+0.027}_{-0.024}$
$\theta_{12}(^\circ)$	$33.67^{+0.73}_{-0.71}$	$33.67^{+0.73}_{-0.71}$
$\theta_{13}(^\circ)$	$8.58^{+0.11}_{-0.11}$	$8.57^{+0.13}_{-0.11}$
$\theta_{23}(^\circ)$	$42.3^{+1.1}_{-0.9}$	$48.9^{+0.9}_{-1.2}$
$\delta(^\circ)$	232^{+39}_{-25}	273^{+24}_{-26}

Table 1.1: Present derived parameter values and their uncertainties at $\pm 1\sigma$ standard deviation in the case of normal and inverted orderings [39], [40].

Using those derived parameter values, the norm of the PMNS matrix elements in the 3σ range have been constrained to be:

$$U = \begin{pmatrix} 0.801 \to 0.842 & 0.518 \to 0.580 & 0.143 \to 0.155 \\ 0.244 \to 0.500 & 0.498 \to 0.690 & 0.634 \to 0.770 \\ 0.276 \to 0.521 & 0.473 \to 0.672 & 0.621 \to 0.759 \end{pmatrix}. \tag{1.12}$$

We see in Table 1.1 and in Eq.(1.12) that there are two large angles and the third is not that small. Thus a dominant eigenstate approximation must be ruled out and each mass can not uniquely be attributed to a flavour. The standard notation is to attribute to $|\nu_1\rangle$ the largest component of the electronic eigenstate. Therefore:

- $|\nu_1\rangle$ will interact as an $\nu_e \sim 2/3$ of the time and $\sim 1/3$ of the time as ν_μ or ν_τ,
- $|\nu_2\rangle$ will interact $\sim 1/3$ of the time as any of the three flavours,
- $|\nu_3\rangle$ will interact $\sim 2.5\%$ of the time as an ν_e and $\sim 45\%$ of the time as a ν_μ or ν_τ.

Knowing that, the mass hierarchy problem is illustrated in Fig. 1.4. When neutrinos pass through a dense medium, they can be coherently forward scattered. This effect, known as the Mikheyev-Smirnov-Wolfenstein (MSW) effect, can enhance oscillations. The mass hierarchy is studied thought those matter effects. Present measurements disfavor the IO by 2 to 3 σ compared to the NO.

Let us note an important remark before closing this section. We know from Z decay that only three flavours of neutrinos are expected. Indeed, the total Z partial width is assumed to be due to Z decaying into quarks and charged leptons, which constitutes the visible partial width, and to a contribution of each neutrino involved in weak interactions

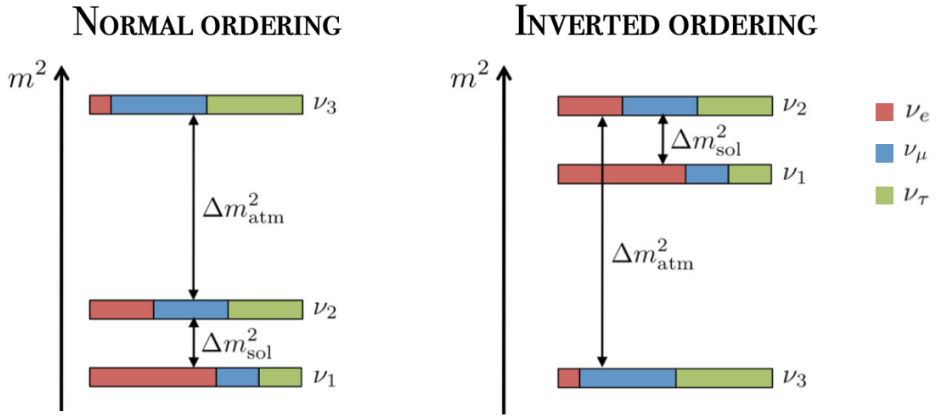

Figure 1.4: Illustration of the mass hierarchy problem, where the normal and inverted ordering are represented. Image taken (and slightly adapted) from [41].

which constitutes the invisible partial width. This latter thus gives the number of neutrinos, N_ν. Combined results from the four LEP experiments with corrections estimate $N_\nu = 2.9963 \pm 0.0074$. Considering three flavour neutrinos, only two mass differences are independent and the actual scheme was complete with previous measurements of two mass splittings.

1.3 Object of this work

In the 1990s, the hypothesis of neutrino oscillations was already proposed as an apparent solution to the solar neutrino problem. The possibility for neutrinos to have a mass would have non-negligible implications. Direct mass measurements are based on kinematic studies and it is difficult to explore low-mass regions, typically $\lesssim 1$ eV^2. As the oscillation principle furnishes constraint on mass squared differences, indirect mass searches started also in oscillation experiments [42]. The *Liquid Scintillator Neutrino Detector* (LSND) experiment was designed to probe the $\Delta m^2 \sim 1$ eV^2 region with a short baseline length of 30 m and typical neutrino energies of 30 MeV. The collaboration first reported an excess of $\overline{\nu}_e$ in 1996 [43]. If those results are interpreted in terms of $\overline{\nu}_\mu \to \overline{\nu}_e$ oscillations they would require the existence of a new mass difference in the $0.2-10$ eV^2 energy range, while no other was expected to be found.

The detector was located at the Los Alamos Neutron Science Center (Southwestern United States) and consisted of a cylindrical tank of 8.3 m length and 5.7 m diameter filled with 167 tons of mineral oil plus a low-concentration liquid scintillator. The inner surface was photosensitive at 25% with 1220 uniformly spaced PMTs and could detect Cherenkov and scintillation light. There was an overburden of roughly 2 kg/cm^2 outside the detector on all sides except the bottom. In addition, there was an external veto region of a 15 cm layer of liquid scintillator with 292 PMTs to track and identify entering cosmic ray muons. It used the Los Alamos Neutron Science Center linear accelerator to produce a proton beam of 800 MeV. The latter passed through a carbon target located 30 m from the center of the detector before reaching a copper beam stop. At those proton energies, the production of kaons and heavier mesons is negligible and plenty of pions and muons decay at rest according to Eqs.(1.1) and (1.2). Produced π^- and μ^- are mainly

absorbed in the copper beam stop and in the shielding. This way, 8 times more π^+ than π^- contributes to neutrino flux production and most of the $\overline{\nu}_e$ flux is suppressed[16]. The resulting flux was simulated to be mostly made of $\overline{\nu}_\mu$ with energies between 20 and 52.8 MeV. To search for oscillations, $\overline{\nu}_\mu$ from μ^+ decay are tracked and $\overline{\nu}_e$ are detected via inverse beta decay and the resulting detection of neutron capture that produces a 2.2 MeV photon. The first time the collaboration observed approximately five times more $\overline{\nu}_e$ than expected [43]. Then, results of the period of operation from 1993 to 1998 reported consistent $\overline{\nu}_\mu \to \overline{\nu}_e$ and $\nu_\mu \to \nu_e$ oscillations that would occur in the $0.2-10$ eV^2 Δm^2 energy range. The mixing probability −that is to say the probability that their results are consistent with the neutrino mixing described above− is $0.264 \pm 0.067 \pm 0.045\%$.

On the other hand, a second similar experiment found no signal; the *KARMEN* [44] −which stands for KARlsruhe Medium Energy Neutrino− experiment was a scintillation colorimeter with a shorter baseline of 17.7 m. Despite that, due to their respective characteristics, these two experiments had their most sensitive regions at different values of Δm^2 and for the lower Δm^2 region probed the LSND was nearly three times more sensitive [45]. Many combined analyses were performed and some scientists pointed out the KARMEN baseline could be a little bit too short and thus cannot completely exclude the LSND anomaly. Nonetheless, the LSND results were quite often disregarded at that time. Given the very little probability of oscillation, a more sensitive successor was needed to confirm the signal. It was the *MiniBooNE* experiment −which stands for Mini Booster Neutrino Experiment− located at Fermilab (United States) which confirmed an unexpected excess in 2009. A detailed experiment description and a summary of its results are the subject of the next chapter. Then, Chapter 3 will be dedicated to the problem analysis.

1.4 Neutrino interactions

Before moving on to the discussion of the MiniBooNE experiment, we present hereafter the various possible neutrino interactions of interest to be detected in it. The experiment used ν_μ and $\overline{\nu}_\mu$ beams with a mean energy of 800 and 600 MeV respectively. This section, based on [6] and [11], presents interactions when considering ν_e, $\overline{\nu}_e$, ν_μ and $\overline{\nu}_\mu$ energies of 0.1 up to 3 GeV.

1.4.1 Charged current quasi-elastic scattering

The predominant neutrino interaction is quasi-elastic scattering, when a neutrino (or antineutrino) elastically scatters off a nucleon from the target through the exchange of a charged W^- (or W^+) boson. The quasi-elastic scattering thus refers to charged current scattering and is often abbreviated as CCQE but we will keep the abbreviation CC throughout this work. In the most simple case it corresponds to the following reactions:

$$\nu_l + n \to l^- + p, \qquad \overline{\nu}_l + p \to l^+ + n. \tag{1.13}$$

[16]For the three first years of data collection, from 1993 to 1995, the target configuration was different. In 1996, with their new target configuration, they could reduced the $\overline{\nu}_e$ background even more. More precisely, the resulting flux ratio of $\overline{\nu}_e$ over $\overline{\nu}_\mu$ was expected to be of $8\ 10^{-4}$ for neutrinos energies between 20 and 52.8 MeV.

where l is the charged lepton associated with the neutrino flavour.

First measurements were done on light targets (*i.e.* hydrogen or deuterium) where the resulting products could clearly be identified. With heavier targets, interactions with nuclei are more complex and nuclear effects can lead to additional particle production. Therefore elastic interactions can imply multiple nucleon productions.

1.4.2 Neutral current elastic scattering

Elastic scattering from neutral current (NC) is an elastic scattering mediated this time by the exchange of a neutral Z^0 boson. We have:

$$\nu + N \to \nu + N, \qquad \overline{\nu} + N \to \overline{\nu} + N \tag{1.14}$$

where N stands for nucleon.

1.4.3 Inelastic scattering

In the following subsections, equations for antineutrinos are not displayed to reduce the notation but these correspond simply to neutrino conjugated reactions.

Resonant single pion production

In some cases the neutrino can excite a nucleon in the target, typically creating n^*, p^* or a resonance of the Δ particle, that quickly decays. Most often decay products are a nucleon and a single pion. Three CC reactions and four NC reactions participate in these and constitute the dominant single pion production channel. The CC single production pion reactions are:

$$\nu_\mu + N \to \mu^- + N + \pi^+, \tag{1.15}$$
$$\nu_\mu + n \to \mu^- + p + \pi^0. \tag{1.16}$$

And the NC single pion production reactions are:

$$\nu_\mu + N \to \nu_\mu + N + \pi^0, \tag{1.17}$$
$$\nu_\mu + p \to \nu_\mu + n + \pi^+, \tag{1.18}$$
$$\nu_\mu + n \to \nu_\mu + p + \pi^-. \tag{1.19}$$

Here also, the use of heavier target elements increases the complexity of the interaction. In those cases, theoretical simulations of neutrino flux need to account for nuclear effects.

Sometimes instead of decaying into a pion these resonant particles undergo other decay processes. There is radiative decay to photons: $\Delta \to N + \gamma$ and $N^* \to N + \gamma$. It happens less than 1 % of the time but these radiative decays cannot be considered negligible as we will discuss later. At other times these resonant particles decay into several pions and mesons. The dominantly produced particles are pions but the kaons contribution is also

significant. More precisely, in MiniBooNE beams most of the ν_μ (resp. $\overline{\nu}_\mu$) flux produced is due to π^+ (resp. π^-) and subsequent μ^+(resp. μ^-) decay and most of the ν_e (resp. $\overline{\nu}_e$) flux is due to K^+ (resp. K^-), K^0 and μ^+ (resp. μ^-) decays [46]. The branching ratios used in the Monte Carlo flux estimation of the MiniBooNE experiment are presented in Table 2.1.

Coherent pion production

Another possibility is that the incoming neutrino scatters on the nucleus and transfers only a small amount of energy to the target. This way it produces a single coherent pion, distinctly forward-scattered. Both CC and NC processes contribute to those reactions, and respectively are:

$$\nu_\mu + A \to \mu^- + A + \pi^+, \tag{1.20}$$

$$\nu_\mu + A \to \nu_\mu + A + \pi^0. \tag{1.21}$$

where A refers to the target.

1.4.4 Deep inelastic scattering

Deep inelastic scattering happens when the neutrino is energetic enough to interact with nucleon quarks. This generally produces multi-pion. This channel becomes important at about 4 GeV and dominates at higher energies. In our considered energy range it is thus negligible.

Chapter 2

MiniBooNE experiment

The MiniBooNE (MB) experiment was designed to search for $\overline{\nu}_\mu \rightarrow \overline{\nu}_e$ and $\nu_\mu \rightarrow \nu_e$ oscillation signals in the $\Delta m^2 \sim 1$ eV^2 region. With the use of a baseline length of about 550 m, the antineutrino channel was studied with a $\overline{\nu}_\mu$ beam of 600 MeV mean energy whereas the neutrino channel was studied with the use of a ν_μ beam of 800 MeV mean energy. Given that the MB experiment probed neutrinos with energies an order of magnitude higher than the previous LSND experiment, backgrounds and systematic errors are completely different. Therefore its results ensure an independent check of oscillations in this region [47].

2.1 Detector description

This first section is dedicated to a detailed description of the experiment of interest. Information in this section is largely based on the MB Collaboration detailed experiment paper [47], their neutrino flux prediction papers [46][48] and from their published results [49][50][51] to complete the discussion.

2.1.1 General setup description

The apparatus consisted of a 12.2 m diameter sphere separated into two volumes by a 35 cm thick opaque barrier that supports 1280 equally spaced PMTs pointing toward the sphere centre. This way 11.3% of the inner surface is photosensitive. The external volume served as a veto region with 240 PMTs used to track entering and exiting particles. The sphere is filled with 818 tons of pure mineral oil (CH_2) with a low-concentration scintillator. A room was above the detector tank for electronics and utilities. The setup was sheltered in a 13.7 m cylindrical vault and covered by 3 m of dirt overburden as depicted in Fig. 2.1.

It was a Cherenkov detector. As already briefly presented in section 1.1, the phenomenon is illustrated in Fig. 2.2. The emission of light angle θ is defined by

$$\cos\theta = \frac{1}{n\beta} \tag{2.1}$$

where n is the refraction index and β is the ratio of the particle velocity over light speed $\beta = \frac{v_p}{c}$ [11]. Depending on the energy of the particle, the light appears blue or is in a

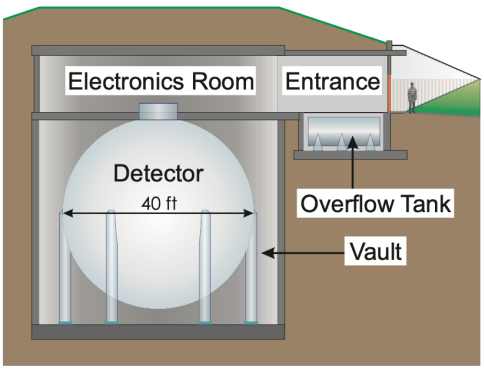

Figure 2.1: Schematic representation of the MB experiment disposition, from [47].

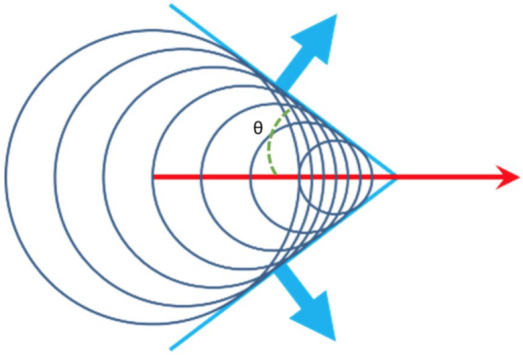

Figure 2.2: Schematic representation of the Cherenkov effect, taken from [52].

shorter UV domain.

For that kind of detector the choice of mineral oil as liquid has some advantages. For the MB experiment it was chosen such that the following requirements were satisfied:

- ▷ at most 25% of the light produced by a neutrino interaction in the tank centre is lost. This way it requires a large extension length in the wavelength of interest. In mineral oil the light attenuation length increases with wavelength such that it reaches a few cm at 280 nm to more than 20 m at 400 nm.
- ▷ there is a small dispersion in the 320 to 600 nm wavelength range to allow better Cherenkov light detection hence event reconstruction.
- ▷ the Cherenkov threshold is lowered to allow the detection of background lower energy particles. It is possible if the speed of light in the medium is lower than in water. Mineral oil has a refractive index of $n = 1.47$ compared to $n = 1.33$ for water.
- ▷ it has low reactivity with the detector materials to reduce most the natural radioactivity in the tank.

What made the greater sensitivity of this experiment is due to

its larger target mass than the LSND experiment. There were about 5 times more mineral oil which permitted to generate much more neutrino interactions. As an illustration, about 1000 neutrino oscillation events were expected as the result of 10^{21} protons on target.

its excellent discrimination between ν_e and ν_μ events. Given the small LSND oscillation probability, the intrinsic neutrino backgrounds had to be clearly identified to limit at most the misidentified excess. This aspect will be discussed in more depth in the second next subsection dedicated to events selection.

its spherical shape that guarantees no dead region in the inner tank. This guaranteed the detection of the two photons from π^0 decay. Without a proper two-photon detection this reaction is not correctly identified and contributes to an increase of the background. The discussion on backgrounds is done in a further subsection.

the presence of a shield from all sides. Unlike the LSND experiment which was not shielded at the bottom.

The PMTs had a wavelength dependent efficiency. Their efficiency peaked at 390 nm and fell to half its maximum at 315 and 490 nm. These had a minimal charge detection of 2 MeV (~ 0.1 photoelectron) and an intrinsic time resolution of ~ 1.5 ns. A digitising system stored the digitised time and integrated charge from each PMT every 100 ns. That information was firstly temporarily stored in a buffer during 200 μs and only signals above the trigger (i.e. for events rejection) were read out. The vault helped to reject cosmic ray muons and the results of neutrino interactions outside the detector. Muons that managed to penetrate the vault were tracked thanks to a scintillator hodoscope. It determined the position and direction of entering muons and its information allowed event reconstruction. In addition there were seven scintillator cubes in the external part of the detector. Each cube was nestled in a sealed aluminum box with an optical fiber connected to a PMT. Those were placed at various distances from the optical barrier to allow the detection of stopping muons from 20 to 800 MeV. Corresponding Cherenkov light and signal in scintillator cubes enables to independently track the muon (and its decay products) trajectory and momentum as it passes through the detector (or decays in it).

2.1.2 Neutrino flux production

The source was made from a proton beam of 8 GeV kinetic energy from the Fermi National Accelerator Laboratory Booster synchrotron. The beam passed through a 71 cm long by 1 cm diameter beryllium target, located 541 m from the detector centre, within a magnetic focusing horn. Depending on its polarity, one could choose to focus positively charged pions and kaons (which is referred to as **neutrino mode** as these are the most dominantly produced) or negatively charged pions and kaons (which is referred to as **antineutrino mode**). Few kaons and plenty of pions are produced and could decay in flight in a 50 m long and 91 cm radius decay pipe. The decay pipe was filled with air at atmospheric pressure. At its end, resulting charged particles were stopped by a 2.2 m thick steel and concrete beam dump and decayed at rest. This thick absorber was used to stop muons and produce the neutrino flux and also contributed to absorb particles apart from neutrinos. Finally, 474 m further, neutrinos reached the detector vault.

The resulting flux properties were based on a Monte Carlo (MC) simulation. This simulation comprised a first part that modeled the initial proton beam properties based on the intrinsic beam optic properties and geometry. A second part modeled the primary proton-Beryllium interactions that generate protons, neutrons, pions and kaons ($K^{\pm}$ and K^0). It took elastic and quasi-elastic scattering of protons in the target into account. A third part simulated how those produced particles propagate up to the detector. It took energy loss, electromagnetic and hadronic processes, decay processes and the impact of the magnetic field into account. The last part consisted of neutrino production simulation based on possible branching ratio decay processes depending on the polarization and its effects. The branching ratios considered as neutrino production decay modes in their simulation are displayed in Table 2.1. Although mentioned in section 1.1, we recall that the π^0 decays rapidly as two photons (i.e. with a mean lifetime of $8.43 \pm 0.13\ 10^{-17}$ s [11])

This way in neutrino mode the flux was expected to be composed at 93.5% of ν_μ, 5.9% of $\overline{\nu}_\mu$, 0.5% of ν_e and lastly 0.1% of $\overline{\nu}_e$. The resulting flux mainly consisted of ν_μ that

Particle	Lifetime (ns)	Branching ratio (%)	Decay mode	Antiparticle	Decay mode
π^+	26.03	99.9877	$\mu^+ + \nu_\mu$	π^-	$\mu^- + \overline{\nu}_\mu$
		0.0123	$e^+ + \nu_e$		$e^- + \overline{\nu}_e$
K^+	12.385	63.44	$\mu^+ + \nu_\mu$	K^-	$\mu^- + \overline{\nu}_\mu$
		4.98	$\pi^0 + e^+ + \nu_e$		$\pi^0 + e^- + \overline{\nu}_e$
		3.32	$\pi^0 + \mu^+ + \nu_\mu$		$\pi^0 + \mu^- + \overline{\nu}_\mu$
K^0_L	51.6	20.333	$\pi^- + e^+ + \nu_e$		
		20.197	$\pi^+ + e^- + \overline{\nu}_e$		
		13.551	$\pi^- + \mu^+ + \nu_\mu$		
		13.469	$\pi^+ + \mu^- + \overline{\nu}_\mu$		
μ^+	2197.03	100.0	$e^+ + \nu_e + \overline{\nu}_\mu$	μ^-	$e^- + \overline{\nu}_e + \nu_\mu$

Table 2.1: Branching ratios and lifetime of secondary particle used in the MC flux production simulation. Data extracted from [46].

peaked at approximately 600 MeV, up to 3000 MeV with a mean energy of $\sim$ 800 MeV. In antineutrino mode the flux was expected to be made of 15.7% of ν_μ, 83.7% of $\overline{\nu}_\mu$, 0.2% of ν_e and lastly 0.4% of $\overline{\nu}_e$. The resulting flux of mainly $\overline{\nu}_\mu$ peaked at approximately 400 MeV and had a mean energy of $\sim$ 600 MeV. Systematic errors in the flux prediction are reported in Table 2.2 together with the corresponding flux variations.

Source of uncertainty	Neutrino mode				Antineutrino mode			
	ν_μ	$\overline{\nu}_\mu$	ν_e	$\overline{\nu}_e$	ν_μ	$\overline{\nu}_\mu$	ν_e	$\overline{\nu}_e$
Proton delivery	2.0%	2.0%	2.0%	2.0%	2.0%	2.0%	2.0%	2.0%
Proton optics	1.0%	1.0%	1.0%	1.0%	1.0%	1.0%	1.0%	1.0%
π^+ production	14.7%	1.0%	9.3%	0.9%	13.8%	0.1%	2.1%	0.1%
π^- production	0.0%	16.5%	0.0%	3.5%	0.5%	17.5%	0.0%	13.6%
K^+ production	0.9%	0.2%	11.5%	0.3%	3.1%	0.0%	22.3%	0.4%
K^0 production	0.0%	0.2%	2.1%	17.6%	0.1%	0.0%	6.1%	3.9%
Horn field	2.2%	3.3%	0.6%	0.8%	1.5%	1.0%	3.2%	1.5%
Nucleon cross sections	2.8%	5.7%	3.3%	5.6%	6.2%	2.1%	6.2%	2.5%
Pion cross sections	1.2%	1.2%	0.8%	0.7%	1.5%	1.2%	1.6%	1.5%

Table 2.2: Systematics errors and variations in the estimated flux of each neutrino type due to systematic uncertainties. Systematics errors are obtained by varying simulation parameters within their uncertainties. Data extracted from [46].

The various sources of uncertainties considered proton delivery which concerns the estimation of the number of protons on target. This estimation is itself impacted by the

optics of the proton beam. Then there are the dominant uncertainties related to the particle production rates and spectra. As mentioned in section 1.4, hadronic interactions have many complex effects and their uncertainties is not explicitly written in their tables but is accounted for in the horn magnetic field and pion and nucleon cross sections uncertainties. The horn field uncertainty also encompasses changes in its focusing properties.

The final MC predicted flux is then compared to the observed data to constrain the expected event rates. It serves to constrain the uncertainties in flux predictions and typically reduce them. In addition it allows to know the accuracy of the simulations which were really good as illustrated in Fig. 2.3. The left figure shows the π^0 reconstructed mass distribution as collected from the two first running period in neutrino mode compared to the simulation and the right figure shows the reconstructed neutrino energy distribution for ν_μ CC events as observed in the detector by the two first running periods in neutrino mode compared to the MC simulation. In those figures error bars show statistical uncertainties only[1]. The reconstructed neutrino energy (E_ν^{QE}) is determined assuming a CC event from the lepton energy and angle with respect to the known neutrino direction. The ratio between the number of data observed to predicted of π^0 events is 0.999 and the ratio of the number of data events to predicted of ν_μ CC events is 0.983.

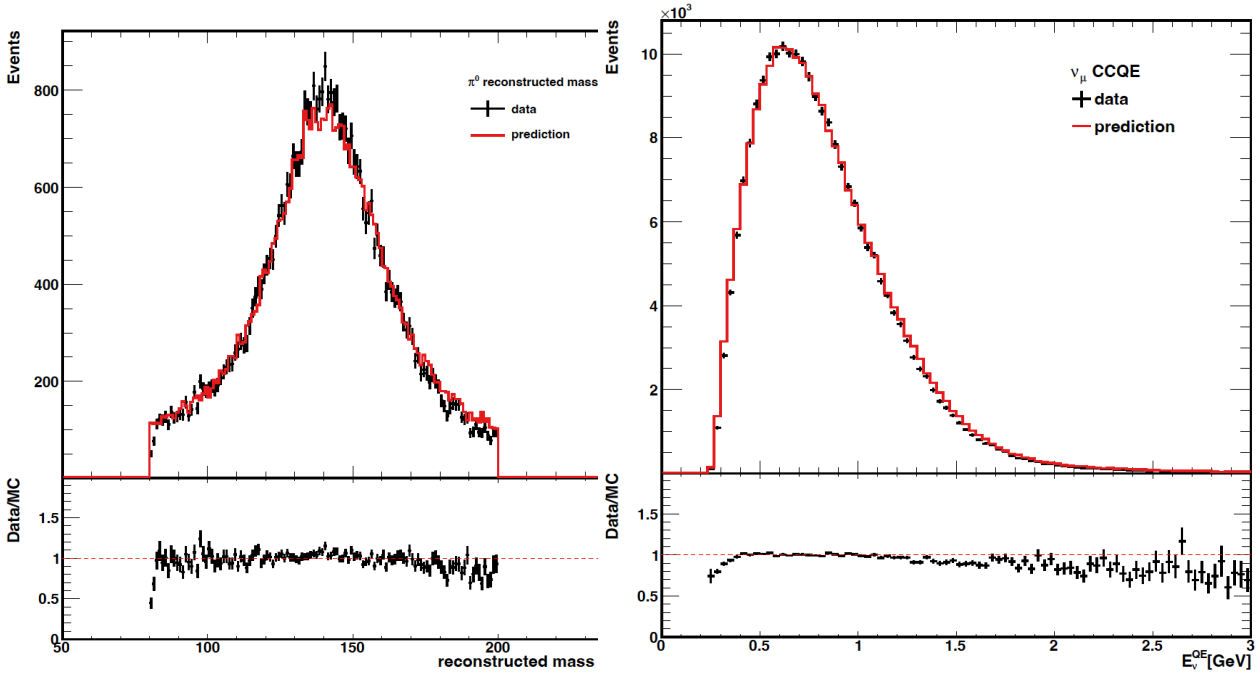

Figure 2.3: The π^0 reconstructed mass distribution (left) and the reconstructed neutrino energy distribution for ν_μ CC events (right) as collected from the two first running period in neutrino mode compared to the MC simulation [53]. Bottom plots show the ratio between the two curves.

In the next subsection we will discuss how events are identified in the detector and selected for the oscillation analysis. This discussion holds for both neutrinos and antineutrinos as PMTs do not distinguish between them. However as mentioned earlier the flux in antineutrino mode contains a non-negligible part of neutrinos contamination ($\sim$ 16 %). In fact despite the focusing horn the very forward pions can escape magnetic deflection.

[1]And this will be the case for the following graphs of this chapter, unless explicitly stated.

This effect has more impact in antineutrino mode because the target choice is such that about twice as many π^+ than π^- are produced, together with neutrino-beryllium cross section that are about three times higher than antineutrino cross section at the studied energy range. Given that the majority neutrino contamination is due to ν_μ produced by the very forward π^+, those are characterised by an angle θ_π with respect to the incoming proton beam < 50 mrad as seen in Fig. 2.4. Consequently the collaboration accounted for the fraction of wrongly signed CC events by determining it from the angular distributions of muons created in those interactions. This method is limited by cross sections and neutrino mode flux uncertainties.

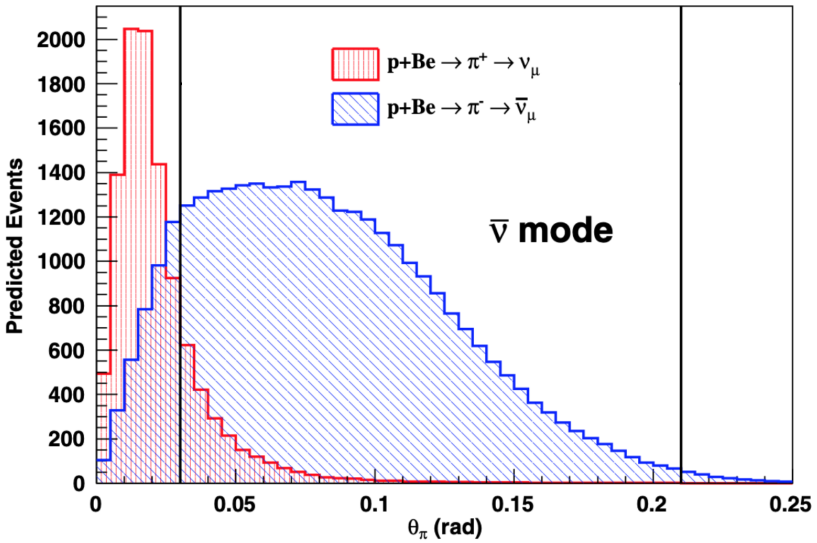

Figure 2.4: Predicted angular distributions of pions in antineutrino mode that produce ν_μ and $\overline{\nu}_\mu$ events in the detector [48]. The θ_π angle is the angle between the pion and proton beam directions.
Note: The central part delimited by black horizontal lines is the part of predicted events for which the collaboration could use pion production data from the HARP experiment for their flux model. We do not enter into such details of the flux models and simulation in this work but the interested reader can find a very complete discussion about it in the detailed papers of the MB collaboration flux production [46] and [48].

2.1.3 Event detection and backgrounds

The possible interactions in the detectors are simulated to be made of

- 39% of charged current quasielastic scattering (Eq. (1.13)),
- 16% of neutral current elastic scattering (Eq. (1.14)),
- 29% of charged current single pion production (Eqs. (1.15) and (1.20)),
- 12% of neutral current single pion production (Eqs. (1.17) and (1.21)),
- <5% for multipion and deep-inelastic scattering contributions.

Consequently particles in the detector are reconstructed to be either a muon, an electron or a π^0. A CC ν_e interaction is tracked back by its electron but this latter is scattered multiple times in water. A CC ν_μ interaction is tracked back to its muon and

its ensuing electron decay sub-event which is observed 80% of the time. Contrarily to electrons, muons rarely interact with water and progressively loose their energy [11]. The Cherenkov light associated to photons is due to water electrons they excite.

On the detector walls the particle track appears as a ring and this way, as illustrated in Fig. 2.5, a CC ν_μ interaction has an associated Cherenkov light which is a succession of clear rings. A single muon-like ring is thus reconstructed as a muon event. On the contrary, a CC ν_e interaction has an associated fuzzy Cherenkov ring traducing its numerous interactions. A single electron-like Cherenkov light is thus reconstructed as an electron event. Lastly, two photon-like rings are associated as a π^0 event. Differences between an electron and a photon signal lie in the fact the electron signal must be correlated in time and place from the reconstructed neutrino interaction which is not the case for photons. Those are allowed to be independently displaced. For a π^0 event the two photons have to have unconstrained kinematics and a total mass equal to π^0 mass.

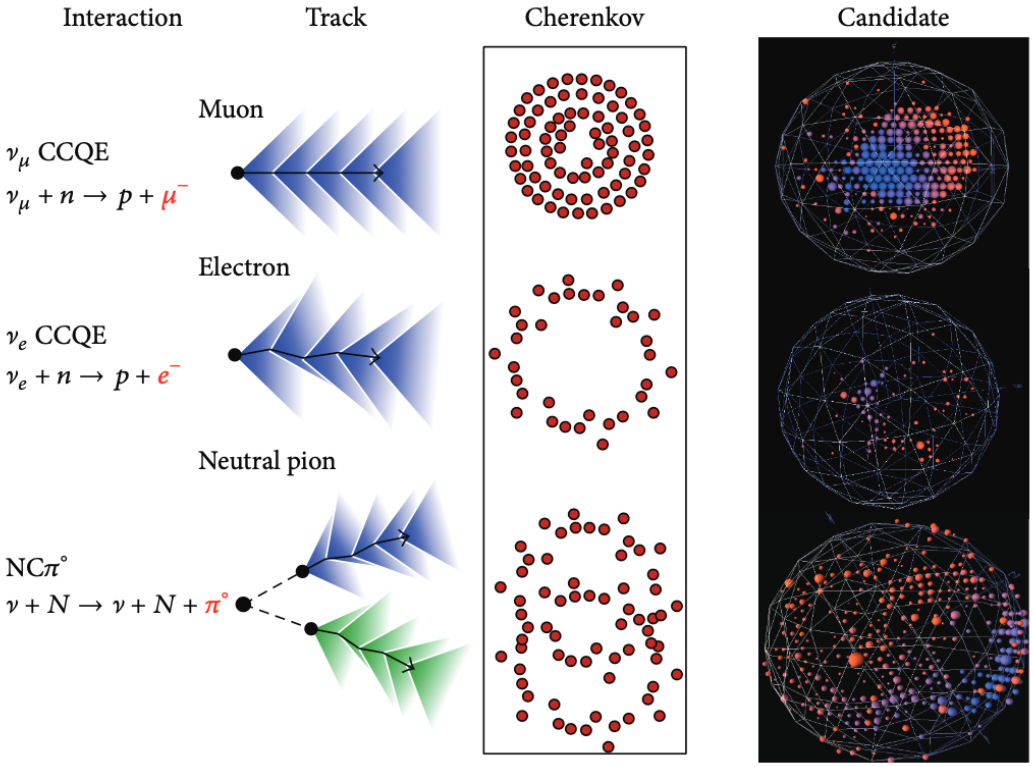

Figure 2.5: Possible events in the MB detector, from [54].

With the use of mineral oil, the velocity of light is lower and contributes to improving the event position reconstruction. In addition the lower dispersion implies there are less multiple scattering hence a less fuzzy ring for electrons. Another point which increases the ν_μ CC reaction identification efficiency is the smaller μ^- capture rate, which is of 8% compared to 20% in water. It means more of them will decay and the particular energy spectrum of the decaying electron ensures a good identification provided that the reconstructed vertex is consistent with the muon track end point. Furthermore the distance between the muon end point and the reconstructed vertex is a function of the reconstructed muon energy. Consequently a ν_μ CC event is characterized by a first sub-event with < 6 PMT veto hits and > 200 PMT hits in the main volume and a second sub-event with < 6 PMT veto hits and < 200 PMT hits in the main volume whose distance is

consistent with the reconstructed vertex. This identification is achieved with 60% efficiency. Each interaction in the tank is precisely detailed by a model that predicts the charge and time of hits on each PMT based on the light propagation and transmission in that particular medium. Algorithms are built to identify clusters and associate the right interaction with the observed event. Finally a maximum likelihood estimation of the observed event allows to reconstruct the interaction vertex properties such as its position and time in the tank, as well as the energy and direction of the incident neutrino. Moreover, as the noise due to bright events exhibits a distinct time structure, algorithms are built to calculate the likelihood associated with a fake sub-event. For electron sub-events of 10 MeV the algorithm efficiency is 99.5% and it increases to 100% when momenta are above 100 MeV. Finally to ensure good event reconstruction and efficiency the electron detection must be at radii < 5 m for ν_e events. For ν_μ events the muon track end point must be at radii < 4.88 m. They also required visible energy to be > 140 MeV where the low-concentration scintillator provides energy information for changed particles produced below Cherenkov threshold. On average the vertex is reconstructed with a position resolution of 22 cm, a direction resolution of 2.8° and an energy resolution of 11% for ν_e events and NC π^0 events are reconstructed with a mass resolution of 20 MeV/c^2.

The resulting beam related background is divided into events induced by ν_e and ν_μ events. The main ν_μ events induced are NC π^0, which are well measured from reconstruction of the two photons invariant mass. Measurements showed these π^0 events have a large tendency to interact near the edge of the imposed internal radius used to reconstruct events which increases the probability of a photon exiting the detector without being detected. With only one photon identified the event could be misidentified as an electron candidate and thus mimic the signal of a ν_e interaction. The second background is radiative Δ baryon decaying into a single photon. Single gamma events are assumed to be only due to these radiative decays. Their estimate of its production rate was in good agreement with other theoretical calculations. Even though these are a few, it is very important to take them into account in models either way these would increase the rate of single photons misidentied as an electron and distort the observed excess. Concerning ν_e backgrounds, these mainly come from μ, K and K^0 decay in the decay pipe and are characterized by a high-energy. Finally, there possibly are neutrino interactions in the surrounding dirt outside the detector. From sample measurements they know these manifest at high radii with low energy inward-pointing events. The presence of other backgrounds is studied by in-situ measurements and data.

Their background predictions were compared with measurements to constraint the predictions. The ν_e CC events induced background has an average selection efficiency of $\sim 20\%$ and is of ~ 0.1 % for ν_μ induced background events.

2.1.4 Event selection and analysis

To lower bias, activity in the detector is recorded 4.4 μs before the arrival of the beam which is on during 1.6 μs. The next $\sim 20\mu s$ there is a beam holdout window that rejects any further trigger to only monitor neutrino interaction inside the detector. Fig. 2.6 illustrates the process of background rejection to obtain a clearer signal for analysis that is to say a signal only due to primary neutrino interactions. In this figure the time distributions of sub-events during a beam-on observation period is shown. The graph (a)

shows all sub-events without cuts. The first flat part is cosmic ray background. The small peak at the beginning is due to the light of passing cosmic rays that occurred just before the trigger of the start of the observation period and was thus not rejected. At about $4.5\mu s$ and during 1.6 μs there is a first sudden electrons rise as $\sim 1 - \exp$ from muon decay as the result of neutrino interactions in the detector. Then there is a flat distribution due to neutrino beam interactions. Finally at around 6 μs, when the beam is off, there is the exponential muon decay electrons fall off. Those low-energy sub-events are characterised by < 200 PMT hits in the detector. Once removed, as seen in graph (b), the distribution of primary neutrino beam interactions appears effectively flat. The last step consists in removing the cosmic rays that entered just after the trigger which are characterised as events with > 6 veto PMT hits. This way the cosmic ray background (and their decay electrons) is reduced by a factor 10^4 as can be seen in graph (c). The veto efficiency is of 99.987% for cosmic ray events above the muon decay electron energy cut-off.

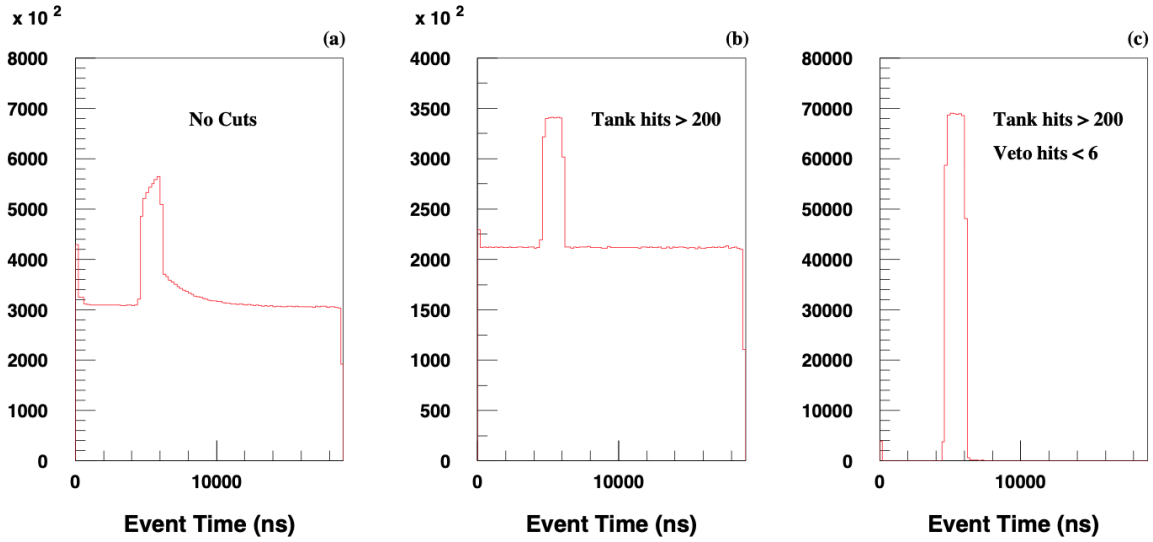

Figure 2.6: Illustration of cosmic ray background and decay electrons rejection of collected events during a beam-on period interval, from [47]. The total period of observation is 19.8 μs. Sub-graph (a) displays all observed events, (b) displays events with lower-energy decay electrons removed and (c) displays the signal with cosmic ray background removed.

After this treatment, event products are carefully analysed to reconstruct the interactions. Their studies showed that once the analysis cuts are made the remaining backgrounds are those related to beam-on interactions.

For data analysis they isolated ν_e CC induced events from a sample. Particle identification algorithms reject ν_μ and π^0 events and their observed rate are used to correct the MC simulation with the appropriate normalising factor.

2.2 Data analysis and results

The MB experiment has collected data from 2002 to 2019. The period of operation consisted of three running periods: from 2002 to 2007, from 2015 to 2017 and lastly from

2017 to 2019. This results in data collection from the interactions of 18.75 10^{20} protons-on-target in neutrino mode and 11.27 10^{20} protons-on-target in antineutrino mode.

The collaboration firstly reported an excess of ν_e CC events in the 200-475 MeV energy range in 2009 [50] and an excess of $\overline{\nu}_e$ CC events in the 475-1250 MeV energy range in 2010 [55]. Their latest result analysis in neutrino mode reported 2870 ν_e CC events observed while the MC simulation predicted 2309.4 ± 48.1 (stat.) ± 109.5 (syst.) events [51] in the 200-1250 MeV energy range which corresponds to an excess of 4.7σ. Their latest result analysis in antineutrino mode reported 478 observed events compared to a prediction of 399.6 ± 20.0 (stat.) ± 20.3 (syst.) events [56]. When they combine both the latest neutrino and antineutrino data, the overall excess of $\nu_e + \overline{\nu}_e$ has a statistical significance of 4.8σ. To interpret the excesses as oscillations, they computed the χ^2 that compares collected data to the predicted background where an oscillation contribution is added. They considered a two-neutrino oscillation and the fit was done for ν_e in the energy range 200 to 1250 MeV. The best fit to the data occurs at $\sin^2 2\theta = 0.807$ and $\Delta m^2 = 0.043$ eV^2. The resulting χ^2 per degree of freedom is 1.4 with a probability of 12.3 %. The computed χ^2 per degree of freedom with the background without an oscillation contribution is 2.93 with a probability of 0.01%.

The associated number of observed events compared to the predicted backgrounds for the latest neutrino mode analysis is shown in Fig. 2.7, together with the best fit to the data. The «other» background comprises mostly neutrino-nucleon and neutrino-electron NC elastic scattering. The fraction of event excess that could be associated to various processes contributing to systematic uncertainties are shown in Table 2.3.

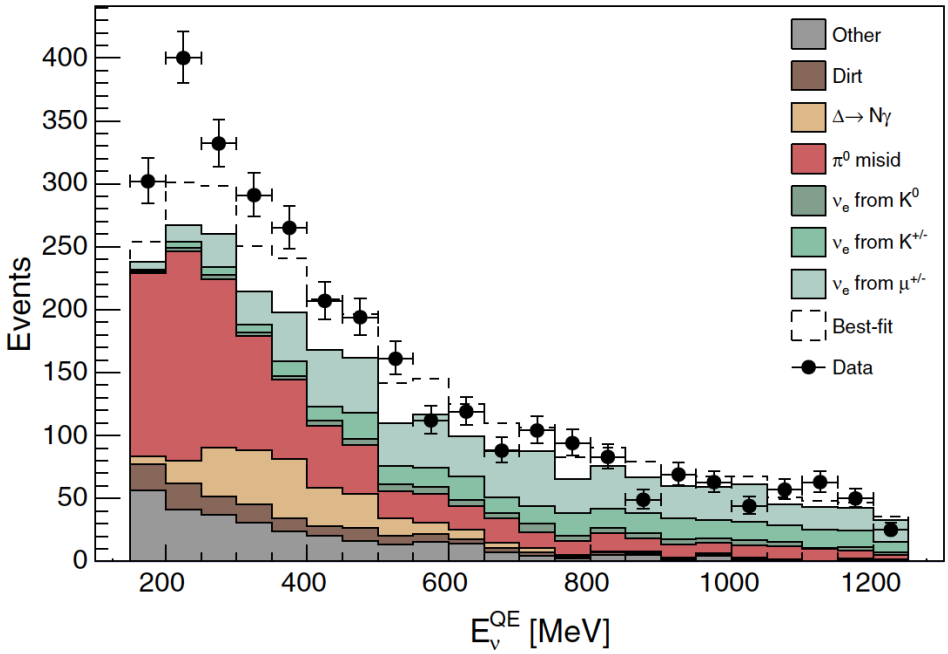

Figure 2.7: Number of ν_e CC events detected in MB depending on the reconstructed neutrino energy E_ν^{QE} in the 150 to 1250 MeV energy range and comprised in a radius of detection less than 4 m. The dashed histogram shows the best fit assuming two-neutrino oscillations [51].

Systematic uncertainty	Fraction of event excess
Cross section	35%
Optical model	23%
π^+ production	14%
Neutrino flux	7%
K^+ production	4%
K^0 production	4%

Table 2.3: Fractional systematic uncertainties of the prediction for 200< E_ν^{QE}<1250 MeV. Data extracted from [51].

Reported excesses in the three running periods in neutrino mode are consistent and appeared for the same neutrino energy range, $\sim$ 200 to 600 MeV, as seen in Fig. 2.8. As a comparison, the reported excess of the antineutrino mode data is shown in Fig. 2.9 with excesses of the combined two first running periods in neutrino mode. The solid curve corresponds to the best fit of both modes at that time which was at $\Delta m^2 = 0.041$ eV^2 and $\sin^2 2\theta = 0.92$, assuming a two-neutrino approximation [53].

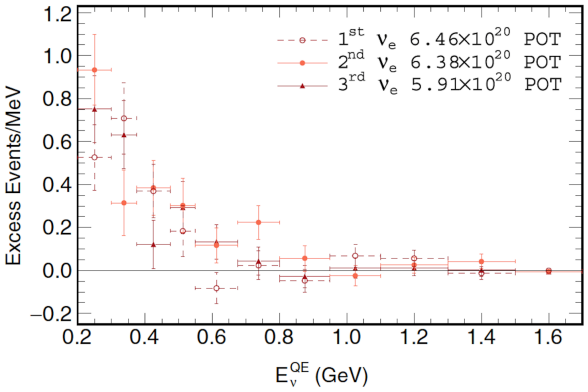

Figure 2.8: Excesses reported for the three running periods as a function of the neutrino energy in neutrino mode, from [51].

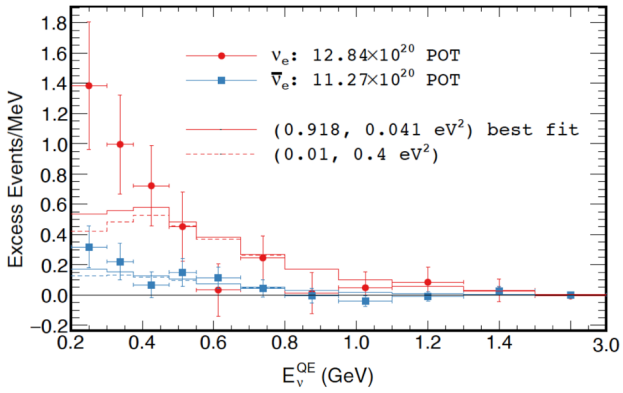

Figure 2.9: Event excesses in antineutrino mode (blue square) compared to the event excess of the combined two first running periods in neutrino mode (red point) [53]. The solid curve corresponds to the best fit of both modes they computed at that time and the dashed curve is the 1σ point best fit. Note that the last bin is for the energy interval 1500−3000 MeV.

Moreover, as they gathered 46% more data in their last analysis in neutrino mode, they performed statistical studies to further investigate the potential origin of the excess. They firstly checked that the excess could not be due to external and NC π^0 event backgrounds. Given the tendency of these reactions to interact in the detector at a high radius, a way to exclude these backgrounds as the origin of the excess is to apply a stronger radius

constraint on the internal volume of detection for the event selection. This way, the resulting analysis performed for events selection with various radii constraints is shown in Table 2.4 as well as its impact on the statistical significance of the excess. The lower limit of 200 MeV was chosen because it is the lowest energy that allows reliable reconstruction of the Cherenkov ring of ν_μ CC events. Nonetheless we see that lowering the energy down to 150 MeV gives the same tendency.

E_ν^{QE} range (MeV)	Radii constraint	Data	Background	Excess	Significance
200 - 1250	$R < 5$m	2870	2309.4 ± 119.6	560.6 ± 119.6	4.7σ
150 - 1250	$R < 5$m	3172	2560.4 ± 131.5	611.6 ± 131.5	4.7σ
200 - 1250	$R < 4$m	1978	1519.4 ± 81.9	458.6 ± 81.9	5.6σ
200 - 1250	$R < 3$m	864	673.9 ± 41.2	190.2 ± 41.2	4.6σ

Table 2.4: Results of the latest neutrino mode MB analysis with various radius constraints [51].

Then, studies of the events radial distribution showed the excess is distributed throughout the volume. Moreover study of beam timing showed that all excesses are correlated in time with neutrino interactions in the detector during beam-on period. Secondly, they tested if their single gamma background was correctly modelled. On the one hand they compared two-dimensional plots of the number of data events, the predicted background events and the excess events as a function of visible energy and the cosine of the angle of reconstructed electron with the incident beam direction. On the other hand, they studied the energy distribution and the electron angle distribution with stronger radii constraint. Both confirmed the background was estimated correctly and agreed with theoretical calculations. In other words, the excess cannot be explained either by external events causing a surplus of non-identified entering photons or wrongly identified π^0 whose one photon is missing because it escaped the detector. Lastly, they tested whether each different background could explain the excess. For this purpose they normalised each of the background radial distribution to the excess radial distribution. Information on the resulting normalising factor needed to match the distributions as well as the resulting log-likelihood fit of two shapes once normalised is shown in Fig. 2.5. The best fit is the one associated to the two-neutrino oscillation hypothesis.

The combined LSND and MB excess has a statistical significance of 6.1σ. Fig. 2.10 shows the L/E_ν^{QE} ratio distributions for the MB data excess in both channels as well as the L/E distribution from LSND. The shaded area is the 1σ allowed band and the dashed curve is the 1σ fit point at $\sin^2 2\theta = 0.01$ and $\Delta m^2 = 0.4$ eV^2. Even if the LSND and MB experiments span the same L/E region, the MB experiment has a larger range of L/E values. To conclude this chapter, we can affirm the MB experiment indeed confirmed the LSND anomaly. According to the excess significance, our current theory cannot explain this surprising result. We investigate the impact of these new results in the next chapter.

Hypothesis	Multiplicative factor	χ^2/9 ndf
NC $\Delta \to N + \gamma$ background	3.18	10.0
External event background	5.98	44.9
ν_e & $\bar{\nu}_e$ from K^0_L decay background	7.85	14.8
ν_e & $\bar{\nu}_e$ from $K^{\pm}$ decay background	2.95	16.3
ν_e & $\bar{\nu}_e$ from $\mu^{\pm}$ decay background	1.88	16.1
Other ν_e & $\bar{\nu}_e$ background	3.21	12.5
NC π^0 background	1.75	17.2
Best fit oscillations	1.24	8.4

Table 2.5: Results of the various tests in order to explain the excess if a multiplicative factor is applied to match the distributions the best together with the resulting χ^2 best fit. Data extracted from [51].

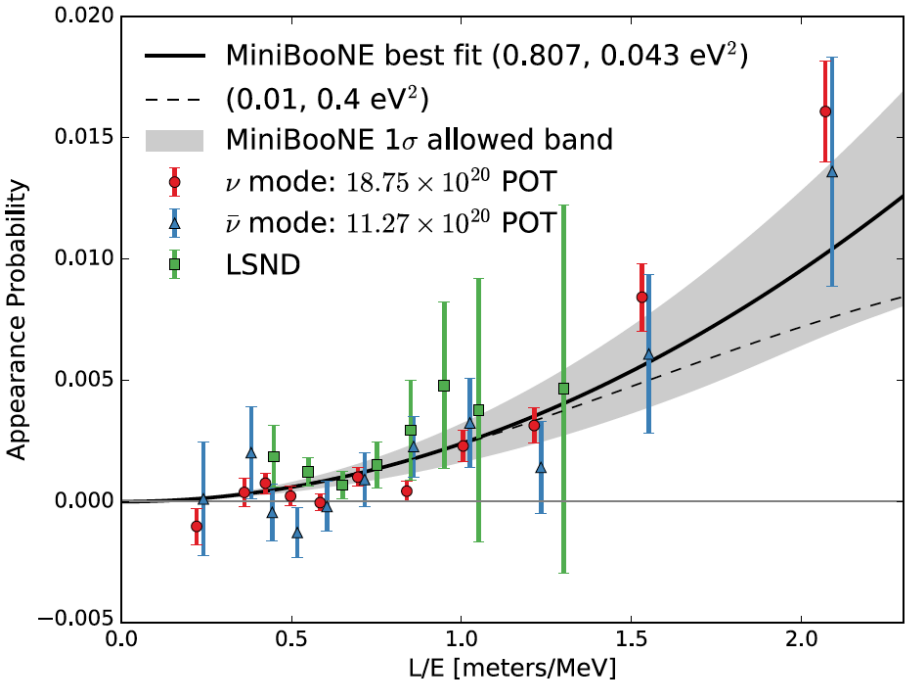

Figure 2.10: Comparison of L/E^{QE}_{ν} distributions of the MB and LSND data [51].

Chapter 3

Problem analysis

This present chapter starts with a simulation to estimate what was expected to be observed by the MB experiment. Then, we will compute the χ^2 in a first approximation and derive the parameter best fit values. We will do it with a data set that does, and does not, consider the MB result. This way we will be able to estimate how it inserts in the current three neutrino mixing scheme. In the second section, we will discuss one of the most investigated solution of this oscillation puzzle; the possible existence of neutrinos still not discovered. The program established to perform the various calculations was done in PYTHON and is available in Annex B.

3.1 Observation versus expectation

In the first instance, let's determine the oscillation rate that was expected to be observed in the MB experiment and compute its standard deviation from expectation. To this aim, we derived the mean oscillation probability that a ν_μ turned into an ν_e by generating 1000 random points in the $\pm 1\sigma$ parameter values interval. The probability was computed by using the previously presented parametrisation of Eq.(1.4) and the present accepted parameters values displayed in Table 1.12. To account for the various energies, each random point generated was evaluated at energies ranging from 200 to 1250 MeV with a path of 50 MeV. One could have also taken baseline length variations into account but given the expected shortest oscillation length L_0^{osci} associated to neutrinos of 200 and 1250 MeV to range from $\sim$ 198 to 1240 km we expect nearly no impact from this consideration. The ν_μ oscillation probabilities as a function of length for a mean neutrino energy of 800 MeV is shown in Fig. 3.1.

Thus the simulation for the 2200 generated point was done with a fixed baseline length of 550 m. The resulting maximum expected probability is 3.3764 10^{-6} and the minimum one is 6.2848 10^{-8} which corresponds to a resulting mean probability of 5.1092 10^{-7} $\pm$ 6.7696 10^{-7} to observe $\nu_\mu \rightarrow \nu_e$ oscillation. As a reminder, the collaboration observed 2870 ν_e events while the expectation was 2309.4 $\pm$ 48.1 (stat.) $\pm$ 109.5 (syst.). Consequently, one would have expected an excess of only 0.00118 ν_e events, while the observed one amounts to 560.6. If we add the errors in quadrature, we retrieve a standard deviation of 4.7 σ, as observed by the collaboration. With such a small probability of oscillations, we understand better that we were expecting to observe none, hence the high deviation of the results.

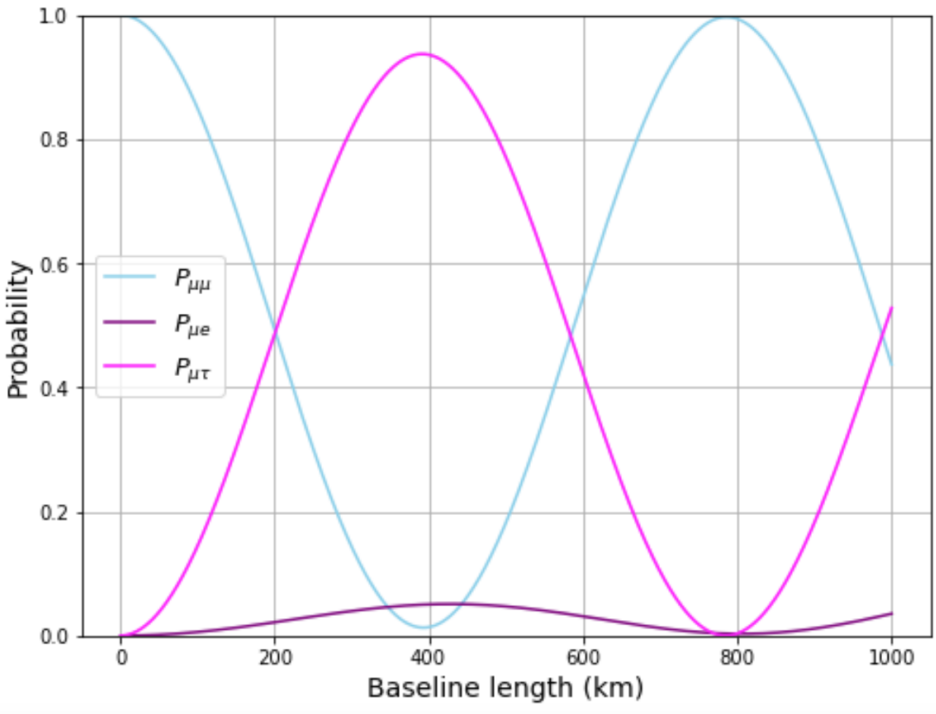

Figure 3.1: Muon neutrino oscillation probabilities as a function of length for a mean neutrino energy of 800 MeV. Its shortest cycle of oscillation happens over 793 km.

Next, we will compute the χ^2 best fit parameters where all the previously presented experiments are considered, then we add the MB result to see how it impacts the fit. The χ^2 statistic is an indicator of the quality of the fit between the data collected and the data as expected by the model and is a weighted sum [11][57]. It is defined as

$$\chi^2 = \sum_i \left(\frac{y_i - y_{i,mod}}{\sigma_i} \right)^2 \tag{3.1}$$

where y_i are the data collected, $y_{i,mod}$ are the data predicted by the model and σ_i are the data errors. Consequently a large χ^2 value ($i.e.$ >> 1) traduces the data are much larger than expected by the model while a small χ^2 value ($i.e.$ << 1) traduces the data are too small compared to the expectation. Here, the expected theoretical values of neutrino fluxes are taken from the 2004 standard solar model of J. N. Bahcall and M. H. Pinsonneault [26]. To account for oscillations in the theoretical expectation, it is implemented in the program as the value expected by theory multiplied by the oscillation probability of interest. That is to say; P_{ee} for solar experiments and $P_{\mu\mu}$ for the atmospheric experiment. For the MB experiment, as we are faced to an excess, it is P_{ee} times the number of ν_e events expected plus $P_{\mu e}$ times the number of ν_μ events expected (which amounts to 107.6 ± 28.2). The observations are the most updated results collected by the experiments previously presented in this work[1], except for the atmospheric experiment. The more recent SK papers furnish the observed data and the expected data as simulated by their model which already take oscillations into account. To be able to use our oscillation probability simulation, we took their first results. However in that paper their

[1]This enables us to consider the SK solar experiment data. Indeed, contrarily to their first measurements, interaction events in the detector have been discriminated between ν_e and ν_μ.

uncertainties are not reported. Based on this review of atmospheric neutrino oscillation discovery [58], we then considered an error on the data of 10%. Lastly, about errors, those are combined in quadrature when needed. When errors are asymmetric, the mean value is taken.

The computation is based on some hypotheses:

- ▷ We consider the normal ordering and we neglect matter effects. We thus consider the neutrino propagates accordingly to the equation valid in vacuum, from its production up to its detection.
- ▷ The incident neutrinos are monoenergetic.
- ▷ For solar experiments, neutrinos are point-produced in the center of the Sun. We do not consider the possibility of the neutrino to be produced at various places inside the Sun's core. This way the distance between neutrino production and detection is approximated as the sun-Earth distance (*i.e.* 149 597 870 700 m [59]) plus the diameter of the Sun (*i.e.* 6.957 10^8 m [60]).
- ▷ For the atmospheric experiment, the traveled distance considered is the average of the Earth's diameter (*i.e.* 1.27562 10^7 m [60]) plus the atmosphere's thickness ($\sim$ 10 10^3 m).

The impact of those hypotheses is discussed a bit further in the text, after the results. The monoenergetic hypothesis enables us to take the mean incident neutrino flux energy depending on the experiment sensitivity. For gallium experiments, we took the middle of the *pp* chain to be 0.3 MeV. Other solar experiments are mainly sensitive to ^8B solar neutrinos, whose mean energy is taken to be 8 MeV. About atmospheric neutrinos, due to the large range of energy their study is separated into sub-GeV and multi-GeV neutrinos. As in the sub-GeV regime neutrinos are more affected by geomagnetic effects we chose to use the multi-GeV data. Those correspond to the $1-10$ GeV range and we thus took thus the mean energy of 5 GeV. All the data, that is to say the data collected, the baseline length and the incident neutrino energy used for the computation are reported in Table 3.1.

In our case we could not use pre-implemented a PYTHON least square regression because, in addition to the oscillation parameters, the probability oscillation function depends on different variables for each data point; the energy of incident neutrinos, the baseline length of the experiment and the flavour change concerned. Therefore we had to implement ourselves the chi^2 function, with the oscillation parameters put as free parameters, and then minimise the resulting function. The minimisation was achieved thanks to the implemented *minimize* module of SCIPY.OPTIMIZE. The inconvenience of that situation is that the optimisation functions return only the value of parameters for which the function is at minimum, with no other information on the fit and hence on their uncertainties.

Experiment	Observation	Expectation	Baseline length (m)	Neutrino energy (MeV)
Homestake	2.56±0.16(stat.)±0.16(syst.) SNU [9]	$8.5^{+1.8}_{-1.8}$ SNU	150293570700	8
SAGE	$65.4^{+3.1}_{-3.0}$(stat.)$^{+2.6}_{-2.8}$(syst.) SNU [61]	131^{+12}_{-10} SNU	150293570700	0.3
GALLEX-GNO	$73.4^{+7.1}_{-7.3}$ SNU [62]	131^{+12}_{-10} SNU	150293570700	0.3
SK (solar)	2.336±0.011(stat.)±0.043(syst.) 10^6 cm^{-2}s^{-1} [63]	5.79±1.33 10^6 cm^{-2}s^{-1}	150293570700	8
SNO	1.70±0.07(stat.)$^{+0.09}_{-0.10}$(syst.) 10^6 cm^{-2}s^{-1} [25]	5.79±1.33 10^6 cm^{-2}s^{-1}	150293570700	8
SK (atmospheric)	230 ν_μ events [29]	295.7 ν_μ events	6383100	5000
MB	2870 ν_e events [51]	2309.4±119.6 ν_e events	550	800

Table 3.1: Data used for the χ^2 computation.

We performed the optimisation with methods that do not require the Jacobean and Hessian matrices to be given as an argument. Their following general description is largely based on this book [64] and on the SCIPY.OPTIMIZE documentation[23].

Nelder-mead It consists of a *simplex downhill method* [65]. In other words, this is a generalised figure with N+1 peaks, where N is the dimension of the problem as a convention throughout this chapter. At each iteration, the highest peak value descends progressively. The new peak point is determined by a reflection with respect to the centroid of all the points, except the highest. This new point is chosen as a new peak if its associated function value is smaller. It does so up to a point where the simplex contracts to its minimum *i.e.* the difference between the function evaluated at each peak and the function evaluated at the centroid is less than a certain fixed tolerance. The minimum value of the function is returned as the value at the centroid. In the simplex descent, if no point is smaller then a new simplex is formed around the lowest peak and it continues. It is the simplest method as the only information contained by the program are the points where the function is evaluated. This method can converge quite quickly thanks to two of its features:

1. if the new peak turns out to be the new lowest value, then the search for a new point is expanded in that direction. If the second new point does not return a lower value, it is simply the previous found that is kept.
2. there is a comparison of the value $\sqrt{\frac{\sum(y_i-\overline{y}^2)}{N}}$ at each iteration, where y_i is the value of the function evaluated at each of the simplex peaks and $\overline{y}$ is the value of the function evaluated at the centroid. If the difference stays at similar large values, then the procedure stops because this situation is associated to a minimum slight curvature. If not, the minimum curvature is steep and it continues its search.

Powell It consists of a *conjugated direction method*. That method performs a successive minimisation of the function with respect to one parameter at a time along conjugated direction vectors *i.e.* conjugated vectors that give the direction of the descent. Indeed for the successive minimisation over each parameter to be conserved, one must have a displacement in a direction that keeps its gradient perpendicular to the current direction. Direction vectors created in such a way are said conjugated. Its main property is that it converges in N step.

Conjugated Gradient (CG) As its name suggests, it is based on a *non-linear conjugate gradient* method. The principle is similar to the previous method, except that here the N conjugated vectors differ at each iteration. The new set of vectors is constructed as a linear combination of the steepest descent direction, based on the approximation of the gradient of the function, and the previous direction. This algorithm is recommended for large problems as it does not use much storage (however more than the first two); just a few vectors and the gradient computation. However on smaller problems rounding errors can become important.

[2]Accessible at : `https://docs.scipy.org/doc/scipy/reference/generated/scipy.optimize.minimize.html#id21`

[3]Furthermore the interested reader about the exact variant method type implemented can found it out at the bottom page of the SCIPY.OPTIMIZE documentation, together with corresponding references of interest.

BFGS It is a *quasi-newton method* that is to say a method that approximates the inverse of the Hessian matrix based on the estimation of the function gradient. Its approximation is updated at each iteration to account for any changes in the curvature measured in the last step. This method thus works until the norm of the gradient is superior to a given tolerance.

TNC This is a *truncated Newton algorithm* [66]. Its difference from the quasi-Newton method relies on the fact that the descent direction interpolates between the steepest descent direction and a modified Newton direction that may be more suitable for large problems. A Newton direction is set by the vector that minimises the second-order Taylor approximation of the function. This direction is reliable when the difference between the true function and its quadratic model is not too large. The qualifier «truncated» stands for the fact that it runs for a limited number of iterations.

COBYLA stands for *Constrained Optimization BY Linear Approximation* method. Thus the algorithm solves a linear approximation of the function at each iteration. It is done inside a *trust region*; a maximum distance region to move on based on a model function. That model function reproduces the actual function based on its behaviour at the current point. Once in that trust-region, it re-do the calculation to estimate the descent path. This method is effective when most of the constraints are linear because constraints are approximated linearly.

SLSQP stands for *Sequential Least SQuares Programming* method which models the function and its constraints at the current iterate by a quadratic approximation of the Lagrange function of the problem. The minimiser of this approximation is then used to define the next iteration.

trust-constr is a sequential least squares trust region method.

Among those methods, the Nelder-mead, the Conjugated gradient and the BFGS methods do not support bound constraints. For the other methods, and for the first χ^2 computation, the bounds used were such that $10^{-6} < \Delta m^2_{12} < 1$, $10^{-4} < \Delta m^2_{23} < 1$ and $0 < \theta_{ij} < \pi$. For the second χ^2 computation, bounds on masses were changed to: $10^{-3} < \Delta m^2_{12} < 1$, $10^{-7} < \Delta m^2_{23} < 1$. Given there are only 6 data points for 6 unknowns, we decided to set the δ phase to zero in the program to enable a better optimisation. Strictly speaking, it has no impact on the other parameter values as the phase cannot be measured directly in oscillations. It is through comparison studies of neutrinos and antineutrinos oscillations that the possibility of CPT violation is investigated. Moreover, it remains the most uncertain parameter. It is thus a convenient choice to help the program by reducing one dimension.

A second point to pay attention to help the minimisation process is a suitable starting point for the parameters. For the first χ^2 computation, the initial parameters were chosen such as $\Delta m^2_{12} = 10^{-4}$, $\Delta m^2_{23} = 10^{-2}$, θ_{12} and $\theta_{23} = 0.8$, and $\theta_{13} = 0.3$. For the second computation, the initial parameters we set as follows: $\Delta m^2_{12} = 0.1$, $\Delta m^2_{23} = 1$, $\theta_{12} = 0.6$ and θ_{23} and $\theta_{13} = 0.8$.

Results of the first minimisation are displayed in Table 3.2 and results of the second minimisation are displayed in Table 3.3.

Method	χ^2	Δm^2_{12} (eV^2)	Δm^2_{23} (eV^2)	θ_{12} (rad)	θ_{13} (rad)	θ_{23} (rad)
Nelder-mead	$4.158\ 10^{-7}$	$5.254\ 10^{-5}$	$2.219\ 10^{-3}$	0.631	0.148	0.754
Powell	$1.604\ 10^{-8}$	$3.705\ 10^{-4}$	$6.220\ 10^{-2}$	0.782	0.263	0.800
CG (*)	$1.189\ 10^{-8}$	$7.693\ 10^{-5}$	$9.966\ 10^{-3}$	0.699	0.149	0.799
BFGS (*)	$9.044\ 10^{-7}$	$8.564\ 10^{-5}$	$9.960\ 10^{-3}$	0.700	0.150	0.799
TNC	$2.097\ 10^{-7}$	$9.806\ 10^{-5}$	$9.956\ 10^{-2}$	0.649	0.149	0.80
COBYLA	5.481	$7.338\ 10^{-3}$	-0.028	1.599	0.160	0.681
SLSQP	$4.822\ 10^{-7}$	1.85410^{-5}	$9.874\ 10^{-3}$	0.796	0.285	0.794
trust-constr (*)	$1.431\ 10^{-10}$	0.446	0.225	0.813	0.369	0.813
Current parameters 3σ allowed range		$6.81 \rightarrow 8.03\ 10^{-5}$	$2.426 \rightarrow 2.586\ 10^{-3}$	$0.551 \rightarrow 0.627$	$0.143 \rightarrow 0.155$	$0.696 \rightarrow 0.891$

Table 3.2: Best fit parameter values and the associated χ^2 given by the various methods tested when the MB results are not considered. The last row displays the derived 3σ range of current parameter values as derived by the NuFit collaboration [39],[40]. Methods marked by an asterisk means that an error message was returned and the optimisation stopped. Only three significant numbers were kept.

Method	χ^2	Δm^2_{12} (eV^2)	Δm^2_{23} (eV^2)	θ_{12} (rad)	θ_{13} (rad)	θ_{23} (rad)
Nelder-mead	21.970	0.029	-0.047	0.626	1.570	0.841
Powell	21.970	0.031	$4.429\ 10^{-5}$	0.570	1.570	3.141
CG	21.970	0.013	-0.010	0.605	1.570	0.805
BFGS	21.970	0.595	-0.621	0.547	1.570	0.887
TNC	21.970	0.001	$1\ 10^{-6}$	0.687	0.559	0.861
COBYLA	21.970	0.393	-0.401	0.667	1.570	0.847
SLSQP	21.970	0.001	$1.038\ 10^{-6}$	0.690	3.141	3.141
trust-constr (*)	21.970	0.124	0.474	0.620	1.570	0.857

Table 3.3: Best fit parameters and associated χ^2 value given by the various method of minimisation when the MB results are added to the data set. Method marked by an asterix means that an error message was return and the optimisation stopped. Only three significant numbers were kept.

When evaluated at the current best-fit parameter values, the χ^2 function without the MB data returns a value of 4.22 10^{-7} whereas the function with the MB data returns a χ^2 value of 22.04. For the first computation, we were expecting a $\chi^2 \sim 1$; its very small value may be accounted as the small number of data points compared to the number of parameters.

In Tables 3.2 and 3.3, methods marked with an asterisk ($*$) means that an error message was returned. For the first computation, both the CG and BFGS method returned an error message concerning the precision which was; `Desired error not necessarily achieved due to precision loss`. This message was returned even when the imposed tolerance for the gradient norm is set to be lower than 10^{-9} to allow for termination. Changing the initial parameter values to a point closer to the expected best fit did not change the situation; the algorithm just stopped the minimum search. The trust-constr method message was `delta grad == 0.0` for both the first and second χ^2 minimisation. Thus this method seems not adapted to our problem. Also, the COBYLA gives a poor fit so the linear approximation seems not well adapted either.

For the first computation −if we disregard the COBYLA and trust-constr methods− the χ^2 value returned is nearly identical for all minimisation. This way the dispersion of the parameter values can give an idea of their errors. As a comparison, the present 3σ region allowed for each parameter is reported in the last row of Table 3.2. Our derivation returned parameter values that are often outside of this 3σ region nonetheless the general tendency of the values are respected even with the two methods that reached the precision limit. For the second computation, the χ^2 value is identical for all the minimisation. Again, the dispersion of the parameter values gives an idea of their errors. This way the most uncertain parameter is the second mass squared difference Δm^2_{23}. Those results are to be compared with the MB best fit performed assuming a two-neutrino approximation; $\Delta m^2 = 0.043$ eV^2 and $\theta_{12} = 0.5579$.

Despite a computation made using kind of first-order approximations, we could show that the χ^2 is largely impacted by the addition of the MB result. Our objective was to see how the χ^2 was impacted as well as the oscillation parameters by the discovery of these unexpected short-baseline oscillations. For both χ^2 minimisation we could retrieve the general tendency expected for the parameter values which fulfill our objective of seeing the impact of the addition of the unexpected excess at short-baseline in our current scheme. We can see that it has a non-negligible impact on the χ^2 value and the new set of mass squared differences retrieved are completely enable to explain the solar and atmospheric experiments. Consequently we see that, if this unexpected signal is interpreted as an oscillation signal, our actual scheme struggles to include them. Of course, we should have derived a more realistic probability function that is to say one that considers the entire energy range of the incident neutrino fluxes, that takes into account the distance production in the Sun and the matter effects both in the Sun and in the Earth (as detectors are underground) but this computation had the purpose of giving an insight of the importance of the problem. With such a deviation in the parameters, we did not expect that more realistic approximations would manage to solve the problem, even if it would provide a much more accurate fit. Such a complete study would be interesting with a higher data set, comprising the most recent experiments performed in accelerators and reactors that obtained much more precise measurements of the parameters. Furthermore, it is difficult to test the impact of the hypotheses we made for our derivation given that

to be able to talk about the errors in distance estimation we would also need to consider the matter effects. Indeed, given solar experiments have a baseline length much larger than the oscillation length, the measured probability P_{ee} is rather an averaged probability that equals $1 - \frac{\sin^2 2\theta_{12}}{2}$. Thus, what allows scientists to derive a proper value of the Δm^2_{12} that generates the oscillations is a joint analysis with the conditions imposed by matter effects in the Sun. As those are not treated here, we will not extend the discussion further. Nonetheless, even without entering into details we can tend to have a general view of the impact of matter effects in our derivation. This effect has been extensively studied and the ν_e survival probability as a function of energy and mater effects could have been established. It turns out that for the *pp* neutrino chain, the P_{ee} equals roughly 0.6 and for the ^8B neutrino chain $P_{ee} \sim 0.3$ [11][1]. If we add a multiplicative factor in the oscillation function implemented in the program such that the derived probability for gallium experiments equals 0.6 and 0.3 for the other solar experiments; the ratio of the new χ^2 over the old, both evaluated at the present parameters values, amounts to 1 for both χ^2 computation. We expect thus to retrieve the same tendency as derived previously.

Before closing this section, let us note the existence of two other short baseline anomalies that support strong evidence that our actual neutrino scheme is incomplete or incorrect. First, the *Gallium anomaly*, which refers to the disappearance of ν_e during the calibration phase of the GALLEX and SAGE collaborations [67]. The GALLEX collaboration tested the detector detection with an artificial ^{51}Cr radioactive source and the SAGE collaboration performed calibrations with a ^{51}Cr and with a ^{37}Ar radioactive source near the detectors. If both results are considered, the statistical significance of the deficit is about 3σ [68]. Secondly, there is the *reactor antineutrino anomaly* that refers to several reactor experiments, whose baseline is less than 100 m, that observed a deficit of $\overline{\nu}_e$ [69].

3.2 Sterile neutrinos

The excess reported by the MB experiment was further investigated by the *MicroBooNE* experiment [70], still at Fermilab. This experiment is a detector that contains 100 tons of liquid argon. It studied oscillations on the eV-mass scale region with a baseline length of 470 m and an incident neutrino beam with a mean energy peaking at 700 MeV. It is a *Liquid Argon Time Projection Chambre* detector, constituted by a cathode plane on one side of the detector and of one anode wire plane at the opposite side. A voltage is set at the cathode plane so that an ambient electric field is created. As a result of a neutrino interaction the charged particle produced in the liquid argon will ionize electrons along its track. The presence of the electric field forces those particles to drift parallel to the field that are collected by wire planes at the end of the volume detector. Due to the high purity of argon, the ionized particles can drift over long distances with minimal attenuation up to wire plans. In addition, the interaction with argon produces scintillation light. The combined information of the light detected, the absolute time of the event and the collected drifted electrons enables a 3D track reconstruction. As the MB experiment could not distinguish an electron event from a single photon, these background sources have been studied in MicroBooNE whose first purpose was to explore the origin of the excess. By studying the average energy deposition at the start of the ionization track, the MicroBooNE experiment can distinguish between electrons and photons. It operated

from 2015 to 2021 and its studies could not explain the MB excess as a result of misidentified photons or electrons [71] which reinforced beliefs in theories based on interactions beyond the standard model. Among those possible interactions, the most investigated is the existence of *sterile neutrinos*.

The following discussion is mainly based on [72] and [73]. The easiest way and also the most instinctive way to solve the current neutrino oscillation problem −that is to say if we extend our actual comprehension of them− is to associate a new particle at this new mass difference to explain the oscillations. It is called *sterile* neutrino because it takes part in the neutrino mixing (and shares the neutrino properties) but is not sensible to weak interactions as it is invisible for the Z decay. It would interact with matter only via gravity. As the new mass squared difference is expected in the 1 eV^2 region, the new mass eigenstate is supposed to be on the order of 1 eV. Numerous derivations including sterile neutrino in the formalism have been done[4]. As there are no restrictions on the number of sterile neutrinos to be involved, some performed models that treat the case of 2 or 3 sterile neutrinos[5]. A combined analysis of the MB and MicroBooNE data has been done by the collaboration [76]; it turns out the model of 3+1 neutrinos has a better fit to the MB data than the model of no oscillations but is still not a suitable model. In fact, up to now, no model has succeeded to fit all the data. Alternative models also treat the case of decaying sterile neutrino but again, these models tend to explain only the MB excess.

Because the electroweak force violates parity, the electroweak interaction couples only to left-handed particles and right-handed antiparticles. It has been pointed out that right-handed neutrinos could act as sterile neutrinos but it would remain to determine why these are invisible for the Z decay. Even if the sterile neutrino hypothesis is the mostly used to explain the short-baseline anomalies, we in fact know nearly nothing about them. Furthermore, there exist other propositions of sterile neutrinos but of much higher energies that could be related to still undetected particles, like for example to those of dark matter. In fact, any other non-standard interaction could interact in some way with neutrinos and act like what we call «sterile neutrinos». Whatever the source of this supposed new interaction, experiments designed to search for hints of sterile neutrino existence have two goals; first those need to prove their existence. This new interaction is tracked by any deviation in the oscillation probability. Their second goal is to obtain precise oscillation measurements to be able to constrain the properties of the underlying phenomena. As this solution track has been proposed for many years, some experiments have already been conducted and could so far only tend to reject the simplest 3+1 model $-i.e.$ these with only one additional sterile neutrino−. But various alternative theories have been proposed and are waiting for new data experiments to be compared with.

[4]See for example this paper [74] of the SK collaboration that interpreted the atmospheric neutrinos deficit as the result of oscillations of muon neutrinos into sterile neutrinos.

[5]as for example in [75], or otherwise numerous other studies with 1, 2 or 3 sterile neutrinos are cited in the reference [73].

Chapter 4

Present and future investigations

The existence of a mass for neutrinos was a notable discovery in particle physics; this was the last time the standard model was modified. Nowadays neutrinos are used as part of multi-messenger and neutrino astronomy to seek beyond the observable of electromagnetic radiation. Therefore knowing better their properties is easily understood to be of great importance. We shall mention another field impacted by neutrinos; Cosmology [11]. In the Big Bang model, neutrinos would have decoupled from matter very quickly, much before the decoupling of photons aftermath of the *recombination epoch* −when protons and electrons could bind and form neutral atoms−. The resulting cosmic neutrino background, also called *relic neutrino background*, has thus participated in the early universe and in the large-scale structure evolution. Those relic neutrinos have not been observed yet nonetheless many of their predictions have been. The impact of neutrino mass in this field is still investigated and direct detection experiments are planned whose data will furnish complementary information to those obtained in particle physics. This stimulating topic is far beyond this work and the interested reader can find a complete discussion in the review [77] and in the «Neutrinos in Cosmology» review of the Review of particle properties [11].
Due to their importance in physics, neutrinos are vastly studied and this has been reinforced in recent years since the reports of short-baseline anomalies. Meanwhile, many theories based on interactions beyond the standard model have been proposed to solve this problem. In this chapter, we will present the experiments planned to investigate the short-baseline excesses which mostly search for hints of sterile neutrinos. Some of them are also expected to investigate the possibility of other new theories.

The surprising excess reported by the MB experiment is currently further studied by the *Fermilab short-baseline neutrino program* [78][79]. This program consists of three Liquid Argon Time Projection Chambre detectors that will focus on ν_e appearance and ν_μ disappearance in the Fermilab Booster Neutrino Beam. Among those three detectors, there is the *Short-Baseline Near Detector* (SBND) located 100 m from the target beam. This detector has started operation in February 2024. Then at 470 m from the target beam there is the MicroBooNE detector that has been mentioned previously. Lastly, there is the *ICARUS T600* detector, 600 m further away from the target. It is also the largest; it contains 500 tons of liquid argon which is $\sim$ 6 times the volume of MicroBooNE and $\sim$ 4 times the volume of SBND. It started operation tests in 2021. It is also the only one underground (but only at shallow depth), both others being at ground level. These have a few meters overburden and a cosmic ray tracking system made of two layers of plastic

scintillators.

The advantage of such liquid argon detectors is their 3D track as well as their higher density that enables more interactions. As mentioned earlier, these are very efficient at electrons-photons events discrimination by measuring the energy deposit along the particle's track. With such large detectors, this is expected that 99% of the LSND proposed region for a new mass squared difference will be explored with more than 5σ significance. Another improvement in the next generation detectors comes from upgrades in beams; they use short-pulsed beam which allows to reduce the time interval of event observation in the detector. This ensures them to observe only neutrino interactions as they can reject better the other particles produced in the beam.

The first phase of this program was performed with the investigation of the excess origin at MicroBooNE. The program is currently investigating hints for sterile neutrinos at the eV mass scale with the use of both SBND and ICARUS as near and far detectors. They also expect to test some beyond standard model hypotheses such as CPT violation. The advantage of having similar detector is that any variation in the flux will be identified as most of the uncertainties related to detector efficiency are canceled out as well as the overall flux.

Collected measurements about neutrino-argon interactions by those experiments will serve to constrain and improve future experiments as well, notably the *DUNE* experiment [80] −which stands for Deep Underground Neutrino Experiment−. It will consist of two detectors; one 474 m from the beam target and a second 1300 km further away. The far detector will contain 70 ktons of liquid argon and will be located at more than 1 km underground at the Sanford Underground Research Laboratory (Lead, South Dakota) and will be the world's largest liquid argon particle detector underground. In addition the beam used will be the most intense neutrino beam delivering neutrinos with energies an order of magnitude higher than existing experiments. The combination of large size detector and higher beam allows a significant number of neutrino interactions to be recorded, even for rare processes, which will allow high statistics data. This experiment aims to answer some of the still unresolved mysteries in the particle's field such as the matter/antimatter asymmetry, leptonic CP violation and the unification forces. It will also study supernovae and the formation of neutron stars or black holes. The far detector prototype started taking data in 2018 but the site is still under construction. The experiment is planned to be operational by 2030.

A second experiment currently in operation is led by the Japan Proton Accelerator Research Complex (J-PARC). It consists of the *JSNS*^{2} experiment [81] [82] −which stands for J-PARC Sterile Neutrino Search at J-PARC Spallation Neutron Source−. It searches for sterile neutrinos at the 1 eV mass scale too, in a $\overline{\nu}_\mu$ beam. The detector is located 24 m further away than the target beam. To have precise event discrimination, a maximum of light must be generated in the detector. Thus the experiment consists of 17 tons of gadolinium-doped liquid scintillator which enables a light yield of $\sim$ 8000 photons per MeV. The $\overline{\nu}_e$ created as the result of $\overline{\nu}_\mu$ oscillation will be detected through inverse beta decay process followed by photons resulting from neutron capture on gadolinium. This capture rate process generates higher energy photons on a shorter time compared to the same process on hydrogen. This contributes to reducing the possibly misidentified background coincident with that reaction by a factor 6. The detector is at ground level, surrounded by 31 tons of liquid scintillator in a stainless steel tank to track entering charged particles. It started operation in 2020.

Lastly, the *Hyper-Kamiokande* experiment [83] is under construction and will be an underground water Cherenkov 295 km from the J-PARC beam. It will be located in the Tochibbora mine in Tokai (Japan). Its volume will be 20 times the one of Super-Kamiokande. The inner surface will be covered at 40% with PMTs. For this detector the increasing sensitivity is due by improved new technology photosensors and improvements in the beam. To better constraint flux measurements, near and intermediate detectors are also planned from a distance ranging from 280 m to $1-2$ km from the target. This experiment will not search for sterile neutrinos but will study neutrinos from various sources; from accelerator neutrino beam, the Earth, the Sun and diverse astronomical sources to understand better the evolution of the Universe. The start of operation is planned for 2027.

All those detectors will furnish complementary information and may confirm a hypothesis that was until now only theoretical.

Conclusion

In this work, we reviewed the discovery of neutrino oscillations and presented the short-baseline anomalies, with a focus on the one firstly discovered by the LSND experiment and then further studied by the MiniBooNE experiment. We derived the expected probability of oscillation to be observed at the MiniBooNE experiment and its tiny value confirmed us that no oscillations were expected over such small distances. Then we computed the χ^2 value of solar and atmospheric experiments to derive a first approximation of the oscillation parameter best-fit values. The addition of the MiniBooNE results largely impacted the χ^2 together with the associated oscillation parameter best-fit values. This clearly showed that these results, if interpreted as a neutrino oscillation signal, do not fit in our actual three-neutrino mixing scheme. We then discussed the addition of sterile neutrinos in the actual formalism even if, up to now, no model has succeeded in fitting all the data. Lastly, we presented some present and future experiments in charge to investigate the short-baseline anomalies. Moreover, the planned next generation experiments should enable us to establish the various peculiarities of neutrinos and shed light on some remaining open mysteries such as the mass hierarchy, the possibility of CPT violation and even to test some models of interaction beyond the standard model. Furthermore, any further constraints on sterile or any other non-standard interaction will need to be in agreement with cosmological observations as well.

In the end, after the oscillation phenomenon was proposed as an apparent solution to the solar neutrino problem, we can say that the situation about neutrino properties became clearer for only a short period of time. Nevertheless, the achievement led by J.N. Bahcall and R. J. Davis was tremendous in succeeding in counting solar neutrinos and marked the start of neutrino astronomy. Still vastly used and studied, neutrinos remain at the centre of many open questions and have thus become of high interest for scientists in many fields of search. Those have actually been intensively studied since their discovery but remain quite elusive; for the few answers obtained twice more questions have arisen. The neutrino physics is a vastly growing area and the next generation of experiments planned should eventually provide some answers.

Appendix A

Two-neutrino approximation

Given the closeness of the mass states $|\nu_1\rangle$ and $|\nu_2\rangle$, a *two-neutrino approximation* is often used. This annexe presents the derivation of the oscillation probability in that case. We consider the practical case of oscillation between electronic and muonic neutrino flavours.

In this case the PMNS matrix is simply a rotation matrix with one mixing angle θ. Therefore the flavour eigenstates are related as

$$\begin{pmatrix} \nu_e \\ \nu_\mu \end{pmatrix} = \begin{pmatrix} \cos\theta & \sin\theta \\ -\sin(\theta) & \cos(\theta) \end{pmatrix} \begin{pmatrix} \nu_1 \\ \nu_2 \end{pmatrix}.$$

By using the same notations and approximations used for the flavour state evolution in section 1.2, the Eq.[1.6] becomes

$$\begin{aligned} |\nu_\mu(t)\rangle &= -\sin\theta e^{-i\left(p+\frac{m_1^2}{2E}\right)L}|\nu_1\rangle + \cos\theta e^{-i\left(p+\frac{m_2^2}{2E}\right)L}|\nu_2\rangle \\ &= e^{-i\left(p+\frac{m_1^2}{2E}\right)L}\left(-\sin\theta|\nu_1\rangle + \cos\theta\,|\nu_2\rangle\, e^{i\left(\frac{\Delta m^2 L}{2E}\right)}\right) \end{aligned}$$

where we denote $m_1^2 - m_2^2$ by Δm^2.

Given that $\langle\nu_e| = \cos\theta\langle\nu_1| + \sin\theta\langle\nu_2|$ and that $\langle\nu_i|\nu_j\rangle = \delta_{ij}$, the transition probability of an initial ν_μ to oscillate into a ν_e flavour is thus given by

$$\begin{aligned} P_{\mu e} = |\langle\nu_e|\nu_\mu(t)\rangle|^2 &= \left|e^{-i\left(p+\frac{m_1^2}{2E}\right)L}\left(-\sin\theta\cos\theta + \sin\theta\cos\theta e^{i\left(\frac{\Delta m^2 L}{2E}\right)}\right)\right|^2 \\ &= 2\sin^2\theta\cos^2\theta - 2\sin^2\theta\cos^2\theta\cos\left(\frac{\Delta m^2 L}{2E}\right) \\ &= 2\sin^2\theta\cos^2\theta\left(1-\cos\left(\frac{\Delta m^2 L}{2E}\right)\right) \\ &= \sin^2 2\theta\sin^2\left(\frac{\Delta m^2 L}{4E}\right) \end{aligned}$$

where the argument of the second sinus can be rewritten under a dimensionless form (as was done at the bottom of p.10) such that

$$P_{\mu e} = \sin^2 2\theta\sin^2\left(1.27\frac{\Delta m^2 L}{E}\right). \tag{A.1}$$

This last equation constitutes the oscillation probability within the framework of a two-neutrino approximation. Given the absence of CP violation phase, $P_{\mu e} = P_{e\mu}$.

Finally, for the graph plotted in Fig.1.2 we were looking at the survival probability. This latter is given by $P_{ee} = P_{\mu\mu} = 1 - P_{\mu e}$.

Appendix B

Python program

The notebook starts with some tests performed to check the PMNS matrix computed as well as the probability function. The two other block of codes show the code used for the derivations done in Chapter 3.

```
import numpy as np
import matplotlib.pyplot as plt
import cmath
%matplotlib inline
from scipy.optimize import minimize
```

```
######### MIXING #########
#Used parametrisation of Eq. (1.4)

def PMNSmatrix(t_12, t_13, t_23, delta):
    x = np.array([[1, 0 , 0], [0, np.cos(t_23), np.sin(t_23)], [0, -np.
 ↪sin(t_23), np.cos(t_23)]])
    y = np.array([[np.cos(t_13), 0, np.sin(t_13)*cmath.exp(-1j*delta)], [0, 1 ,␣
 ↪0], [-np.sin(t_13)*cmath.exp(1j*delta), 0, np.cos(t_13)]])
    z = np.array([[np.cos(t_12), np.sin(t_12), 0], [-np.sin(t_12), np.
 ↪cos(t_12), 0], [0, 0, 1]])
    PMNS = (x@y)@z
    return PMNS


def CheckUnitarity(U):
    """
    Check if the matrix (of dimension 3x3) is unitary.
    It returns a boolean

    Parameters:
    ----------
    U : [array] 3x3 matrix
    """
    I = np.array([[1, 0, 0], [0, 1, 0], [0, 0, 1]])
    Uadjoint = np.conj(U).T
    Test1, Test2 = U@Uadjoint, Uadjoint@U

    return np.allclose(Test1, I, rtol=abs(1e-06), atol=abs(1e-08),␣
 ↪equal_nan=False), np.allclose(Test2, I, rtol=1e-06, atol=1e-08,␣
 ↪equal_nan=False)
```

```
######### Present derived parameter values (from NuFit) #########
t_12, t_13, t_23 = np.deg2rad(33.67), np.deg2rad(8.58), np.deg2rad(42.3)
delta = np.deg2rad(232)
m12 = 7.41*(10**(-5))
m23 = 2.505*(10**(-3))
m13 = m12 + m23


#########  MATRIX TESTS #########
# 1. Check adequation with the PMNS matrix present derived values (displayed in␣
 ↪Eq.(1.14))
flavoureigenstate = np.array(['v_e', 'v_u', 'v_t'], dtype=str)
masseigenstate = np.array(['v_1', 'v_2', 'v_3'], dtype=str)
Matrix = PMNSmatrix(t_12, t_13, t_23, delta)

for i in range(3):
    print(flavoureigenstate[i], " = ")
    for k in range(3):
        print(abs(Matrix[i,k])," ",masseigenstate[k])
    print("-------------------------------------")

 #2. Check has orthonormate eigenstates
for j in range(3):
    e = 0.
    for i in range(3):
        e += Matrix[j, i]*np.conj(Matrix[j, i])
    print(e)

#3. Check U is unitary
CheckUnitarity(Matrix)


######### Probability of oscillations #########
def ProbaDev(alpha, beta, U, E, L, m_12, m_23):
    result, proba = 0., 0.
    result2 = 0.
    arg = 1.267*L/E # argument of the exponential

    #Sum for k<j, i.e. of j from 1 to 2 & k from 0 to 1 :
    for j in range(3):
        for k in range(3):
            factor = U[alpha,k]*np.conj(U[alpha,j])*np.conj(U[beta,k])*U[beta,j]

            if (k == 0) & (j == 1):
                terme1 = np.sin(arg*m_12)**2
                terme2 = np.sin(2*arg*m_12)
```

```
                result += factor.real*terme1
                result2 += factor.imag*terme2

            elif (k == 0) & (j == 2):
                terme1 = np.sin(arg*(m_12+m_23))**2
                terme2 = np.sin(2*arg*(m_12+m_23))
                result += factor.real*terme1
                result2 += factor.imag*terme2

            elif (k == 1) & (j == 2):
                terme1 = np.sin(arg*m_23)**2
                terme2 = np.sin(2*arg*m_23)
                result += factor.real*terme1
                result2 += factor.imag*terme2

    if (alpha == beta):
        proba = 1.-4.*result+2.*result2
    else:
        proba = -4.*result+2.*result2

    return proba

######### Random check that the sum of probabilities = 1 #########
#for an initial electronic flavour of 2 MeV over 100 m
y1 = ProbaDev(0, 0, Matrix, 2, 100, m12, m23)
y2 = ProbaDev(0, 1, Matrix, 2, 100, m12, m23)
y3 = ProbaDev(0, 2, Matrix, 2, 100, m12, m23)

print("Oscillation prob e-> e = ", y1,"\n e -> mu = ", y2,"\n e -> tau = ", y3,␣
 ↪"\n and the sum = ", y1+y2+y3)
```

```
######### Expected observations of the MB experiment #########
# Present derived values, placed as [m_12, m_23, t_12, t_13, t_23, delta] :
parameters = np.array([7.41*(10**(-5)), 2.505*(10**(-3)), np.deg2rad(33.67), np.
 ↪deg2rad(8.58), np.deg2rad(42.3), np.deg2rad(232)])

# +1 sigma variation :
Plus = np.array([0.21*(10**(-5)), 0.024*(10**(-3)), np.deg2rad(0.73), np.
 ↪deg2rad(0.11), np.deg2rad(1.1), np.deg2rad(39)])
# -1 sigma variation :
Minus = np.array([0.2*(10**(-5)), 0.026*(10**(-3)), np.deg2rad(0.71), np.
 ↪deg2rad(0.11), np.deg2rad(0.9), np.deg2rad(25)])

def ProbaDev2(alpha, beta, E, L, *params):

    m_12, m_23, t_12, t_13, t_23, delta = params
```

```
    # When fix delta at 0 it becomes:
    # m_12, m_23, t_12, t_13, t_23 = params
    # delta = 0.

    # Mixing matrix computation
    x = np.array([[1, 0 , 0], [0, np.cos(t_23), np.sin(t_23)], [0, -np.
↪sin(t_23), np.cos(t_23)]])
    y = np.array([[np.cos(t_13), 0, np.sin(t_13)*cmath.exp(-1j*delta)], [0, 1 ,␣
↪0], [-np.sin(t_13)*cmath.exp(1j*delta), 0, np.cos(t_13)]])
    z = np.array([[np.cos(t_12), np.sin(t_12), 0], [-np.sin(t_12), np.
↪cos(t_12), 0], [0, 0, 1]])
    U = (x@y)@z

    # Oscillation probability computation
    factor, result, proba = 0., 0., 0.
    result2 = 0.
    arg = 1.267*L/E # argument of the exponential

    for j in range(3):
        for k in range(3):
            factor = U[alpha,k]*np.conj(U[alpha,j])*np.conj(U[beta,k])*U[beta,j]

            if (k == 0) & (j == 1):
                terme1 = np.sin(arg*m_12)**2
                terme2 = np.sin(2*arg*m_12)
                result += factor.real*terme1
                result2 += factor.imag*terme2

            elif (k == 0) & (j == 2):
                terme1 = np.sin(arg*(m_12+m_23))**2
                terme2 = np.sin(2*arg*(m_12+m_23))
                result += factor.real*terme1
                result2 += factor.imag*terme2

            elif (k == 1) & (j == 2):
                terme1 = np.sin(arg*m_23)**2
                terme2 = np.sin(2*arg*m_23)
                result += factor.real*terme1
                result2 += factor.imag*terme2

    if (alpha == beta):
        proba = 1.-(4.*result)+2.*result2
    else:
        proba = -4.*result+2.*result2

    return proba
```

```
######### Generates random intervals #########
UpperLimit = parameters + Plus
LowerLimit = parameters - Minus

param_initial = np.zeros(6)
simu = [] # will stock the data generated into a list to be able to use
            #the .append module, then it will be converted to an array
k = 0 # to count the data generated outside the interval

for j in range(1000):
    for i in range(6):
        param_initial[i] = random()*(UpperLimit[i]-LowerLimit[i]) +␣
↪LowerLimit[i]

        if(param_initial[i] > UpperLimit[i]):
            param_initial[i] = False
    if(False in param_initial):
        k += 1
    else:
        for l in np.arange(200,1251,50):#creates 22bins of energy (with a path␣
↪of 50MeV)
            simu.append(ProbaDev2(1, 0, l, 550, *param_initial))

Simulation = np.array(simu)
print("Generation done with ", (1000*22)-k," generated points.")

######### Statistics on those generated data #########
print("The minimum probability is ",np.min(Simulation))
print("The maximum probability is ", np.max(Simulation))
print("And the mean probability is ", np.mean(Simulation, axis=0))
print("which traduces a std deviation of ", np.std(Simulation, ddof=1))

######### Graph des proba #########
Oscil1bis, Oscil2bis, Oscil3bis = np.zeros(1000), np.zeros(1000), np.zeros(1000)

for i in range(1000):
    Oscil1bis[i] = ProbaDev(1, 1, Matrix, 0.8, (i+1), m12, m23)
    Oscil2bis[i] = ProbaDev(1, 0, Matrix, 0.8, (i+1), m12, m23)
    Oscil3bis[i] = ProbaDev(1, 2, Matrix, 0.8, (i+1), m12, m23)

fig2 = plt.figure(figsize=(8, 6))
plt.ylim(ymin=0)
x2 = np.arange(1, 1001, 1)

plt.plot(x2, Oscil1bis, color='skyblue', label='$P_{\mu \mu}$')
plt.plot(x2, Oscil2bis, color='purple', label=r'$P_{\mu e}$')
plt.plot(x2, Oscil3bis, color='magenta', label=r'$P_{\mu \tau}$')
```

```
plt.xlabel('Baseline length (km)', fontsize=14)
plt.ylabel('Probability', fontsize=14)
plt.grid()
plt.legend(fontsize=13)
```

```
######### Chi squared computation #########
#/!\ Now we fix the phase at 0
parametersdel = np.array([7.41*(10**(-5)), 2.505*(10**(-3)), np.deg2rad(33.67),␣
 ↪np.deg2rad(8.58), np.deg2rad(42.3)])
Lsolar = 149597870700 + 6.957*(10**8)
Latmospheric = (1.27662*(10**7))/2
Pnamedel = np.array(["m_12", "m_23", "t_12", "t_13", "t_23"], dtype=str)

######### Definition of the Chi squarred WITHOUT MB results #########
def Ch12(params):
    result = 0.
    m_12, m_23, t_12, t_13, t_23 = params
    ## Experimental data values in 'data' are presented with the same order as␣
 ↪presented
    ## in the manuscript i.e. [Homestake, SAGE, GALLEX, SK_sol, SNO, SK_atm]
    ## and their corresponding uncertainties are reported in 'data_sigma' array
    data = np.array([2.56, 65.4, 73.4, 2.336, 1.7, 230])
    data_sigma = np.array([0.226, 4.073, 7.2, 0.044, 0.118, 23])

    # This is the same order for the expected data
    model = np.zeros(6)
    model[0] = ProbaDev2(0, 0, 8, Lsolar, *params)*8.5
    model[1] = ProbaDev2(0, 0, 0.3, Lsolar, *params)*131
    model[2] = ProbaDev2(0, 0, 0.3, Lsolar, *params)*131
    model[3] = ProbaDev2(0, 0, 8, Lsolar, *params)*5.79
    model[4] = ProbaDev2(0, 0, 8, Lsolar, *params)*5.79
    model[5] = ProbaDev2(1, 1, 5000, Latmospheric, *params)*295.7

    for i in range(len(data)):
        result = np.sum(((data[i] - model[i])/data_sigma[i])**2)

    return result

######### Definition of the Chi squarred WITH MB results #########
# The function implementation follows the same convention as above

def Ch12_WMB(params):
    result = 0.
    modelBIS = np.zeros(7)
    m_12, m_23, t_12, t_13, t_23 = params

    dataBIS = np.array([2.56, 65.4, 73.4, 2.336, 1.7, 230, 2870])
```

```
    data_sigmaBIS = np.array([0.226, 4.073, 7.2, 0.044, 0.118, 23, 119.6])

    modelBIS[0] = ProbaDev2(0, 0, 8, Lsolar, *params)*8.5
    modelBIS[1] = ProbaDev2(0, 0, 0.3, Lsolar, *params)*131
    modelBIS[2] = ProbaDev2(0, 0, 0.3, Lsolar, *params)*131
    modelBIS[3] = ProbaDev2(0, 0, 8, Lsolar, *params)*5.79
    modelBIS[4] = ProbaDev2(0, 0, 8, Lsolar, *params)*5.79
    modelBIS[5] = ProbaDev2(1, 1, 5000, Latmospheric, *params)*295.7
    modelBIS[6] = ProbaDev2(0, 0, 800, 550, *params)*2309.4 + ProbaDev2(1, 0,␣
↪800, 550, *params)*107.6

    for i in range(len(dataBIS)):
        result = np.sum(((dataBIS[i] - modelBIS[i])/data_sigmaBIS[i])**2)
    return result

######### Minimization #########
x_0 = np.array([0.1, 1, 0.6, 0.8, 0.8])
bnds = (10**(-4), 2.), (10**(-6), 2.), (0., np.pi), (0., np.pi), (0., np.pi)
res = minimize(Chi2_WMB, x0=x_0, method='Nelder-mead')#, bounds=bnds) # add␣
↪bounds when the method supports it

print('Success? ', res.success, '\n', res.message)
print('Chi squarred = ', res.fun)
for i in range(5):
    print(Pnamedel[i], '=', res.x[i], "\t ")


######### Search of the appropriate multiplicative factor to test MSW
test = np.zeros(6)
test[0] = ProbaDev2(0, 0, 8, Lsolar, *parameters)
test[1] = ProbaDev2(0, 0, 0.3, Lsolar, *parameters)
test[2] = ProbaDev2(0, 0, 0.3, Lsolar, *parameters)
test[3] = ProbaDev2(0, 0, 8, Lsolar, *parameters)
test[4] = ProbaDev2(0, 0, 8, Lsolar, *parameters)
test[5] = ProbaDev2(1, 1, 5000, Latmospheric, *parameters)

Want = np.array([0.3, 0.6, 0.6, 0.3, 0.3 ])
Want/test
```

Bibliography

We draw the interested reader's attention to the fact that the vast majority of the articles cited in this work are also available on the open-access archive platform arXiv, accessible at https://arxiv.org.

[1] F. F. Deppisch, *A Modern Introduction to Neutrino Physics*. IOP Concise Physics. Morgan & Claypool Publishers, 2019.

[2] F. Wilson, "Fermi's theory of beta decay," *American Journal of Physics*, vol. 36, pp. 1150–1160, 1968. DOI: 10.1119/1.1974382.

[3] C. L. Cowan, F. Reines, F. B. Harrison, H. W. Kruse, and A. D. McGuire, "Detection of the free neutrino: A confirmation," *Science*, vol. 124, no. 3212, pp. 103–104, 1956. DOI: 10.1126/science.124.3212.103. [Online]. Available: http://www.jstor.org/stable/1751492.

[4] G. Danby, J.-M. Gaillard, K. Goulianos, *et al.*, "Observation of high-energy neutrino reactions and the existence of two kinds of neutrinos," *Phys. Rev. Lett.*, vol. 9, pp. 36–44, 1 1962. DOI: 10.1103/PhysRevLett.9.36.

[5] K. Kodama, N. Ushida, C. Andreopoulos, *et al.*, "Observation of tau neutrino interactions," *Physics Letters B*, vol. 504, no. 3, pp. 218–224, 2001, ISSN: 0370-2693. DOI: 10.1016/s0370-2693(01)00307-0.

[6] J. A. Formaggio and G. P. Zeller, "From ev to eev: Neutrino cross sections across energy scales," *Reviews of Modern Physics*, vol. 84, no. 3, pp. 21–35, 2012, ISSN: 1539-0756. DOI: 10.1103/revmodphys.84.1307.

[7] J. N. Bahcall, "Solar neutrinos. i. theoretical," *Phys. Rev. Lett.*, vol. 12, pp. 300–302, 11 1964. DOI: 10.1103/PhysRevLett.12.300.

[8] J. N. Bahcall, "Solar models: An historical overview," *Nuclear Physics B - Proceedings Supplements*, vol. 118, pp. 77–86, 2003, Proceedings of the XXth International Conference on Neutrino Physics and Astrophysics, ISSN: 0920-5632. DOI: https://doi.org/10.1016/S0920-5632(03)01306-9.

[9] B. T. Cleveland, T. Daily, J. Raymond Davis, *et al.*, "Measurement of the solar electron neutrino flux with the homestake chlorine detector," *The Astrophysical Journal*, vol. 496, no. 1, p. 505, 1998. DOI: 10.1086/305343.

[10] J. N. Bahcall and C. Peña-Garay, "Solar models and solar neutrino oscillations," *New Journal of Physics*, vol. 6, no. 1, p. 63, 2004. DOI: 10.1088/1367-2630/6/1/063.

[11] R. W. et al., "Review of particle physics," *Prog. Theor. Exp. Phys.*, vol. 2022, 083C01 (2022) and 2023 update, 2022. DOI: 10.1093/ptep/ptac097.

[12] R. Davis, D. S. Harmer, and K. C. Hoffman, "Search for neutrinos from the sun," *Phys. Rev. Lett.*, vol. 20, pp. 1205–1209, 21 1968. DOI: 10.1103/PhysRevLett.20.1205.

[13] J. N. Bahcall, M. H. Pinsonneault, and G. J. Wasserburg, "Solar models with helium and heavy-element diffusion," *Reviews of Modern Physics*, vol. 67, no. 4, pp. 781–808, 1995, ISSN: 1539-0756. DOI: 10.1103/revmodphys.67.781. [Online]. Available: http://dx.doi.org/10.1103/RevModPhys.67.781.

[14] T. Kajita, M. Koshiba, and A. Suzuki, "On the origin of the Kamiokande experiment and neutrino astrophysics," *Eur. Phys. J. H*, vol. 37, pp. 33–73, 2012. DOI: 10.1140/epjh/e2012-30007-y.

[15] Y. Fukuda, T. Hayakawa, K. Inoue, *et al.*, "Solar neutrino data covering solar cycle 22," *Phys. Rev. Lett.*, vol. 77, pp. 1683–1686, 9 1996. DOI: 10.1103/PhysRevLett.77.1683.

[16] A. S. Brun, S. Turck-Chieze, and P. Morel, "Standard solar models in the light of new helioseismic constraints. 1. The Solar core," *Astrophys. J.*, vol. 506, pp. 913–925, 1998. DOI: 10.1086/306271. arXiv: astro-ph/9806272.

[17] J. N. Abdurashitov, V. N. Gavrin, S. V. Girin, *et al.*, "Measurement of the solar neutrino capture rate with gallium metal," *Phys. Rev. C*, vol. 60, p. 055 801, 5 1999. DOI: 10.1103/PhysRevC.60.055801.

[18] J. N. Bahcall, M. H. Pinsonneault, and S. Basu, "Solar models: Current epoch and time dependences, neutrinos, and helioseismological properties," *The Astrophysical Journal*, vol. 555, no. 2, pp. 990–1012, 2001, ISSN: 1538-4357. DOI: 10.1086/321493. [Online]. Available: http://dx.doi.org/10.1086/321493.

[19] M. Cribier, W. Hampel, G. Heusser, *et al.*, "Results of the whole gallex experiment," *Nuclear Physics B - Proceedings Supplements*, vol. 70, no. 1, pp. 284–291, 1999, Proceedings of the Fifth International Workshop on topics in Astroparticle and Underground Physics, ISSN: 0920-5632. DOI: https://doi.org/10.1016/S0920-5632(98)00438-1.

[20] M. Altmann *et al.*, "Complete results for five years of GNO solar neutrino observations," *Phys. Lett. B*, vol. 616, pp. 174–190, 2005. DOI: 10.1016/j.physletb.2005.04.068. arXiv: hep-ex/0504037.

[21] S. Fukuda, Y. Fukuda, M. Ishitsuka, *et al.*, "Solar ^8B and hep neutrino measurements from 1258 days of super-kamiokande data," *Phys. Rev. Lett.*, vol. 86, pp. 5651–5655, 25 2001. DOI: 10.1103/PhysRevLett.86.5651.

[22] H. H. Chen, "Direct approach to resolve the solar-neutrino problem," *Phys. Rev. Lett.*, vol. 55, pp. 1534–1536, 14 1985. DOI: 10.1103/PhysRevLett.55.1534.

[23] D. Waller, "Results from the Sudbury Neutrino Observatory," *SLAC Summer Institute on Particle Physics (SSI04)*, vol. Aug. 2-13, 2004.

[24] Q. R. Ahmad, R. C. Allen, T. C. Andersen, *et al.*, "Measurement of the rate of $\nu_e + d \rightarrow p + p + e^-$ interactions produced by ^8B solar neutrinos at the sudbury neutrino observatory," *Phys. Rev. Lett.*, vol. 87, p. 071 301, 7 2001. DOI: 10.1103/PhysRevLett.87.071301.

[25] S. N. Ahmed *et al.*, "Measurement of the total active B-8 solar neutrino flux at the Sudbury Neutrino Observatory with enhanced neutral current sensitivity," *Physical Review Letters*, vol. 92, no. 18, p. 181 301, 2004. DOI: 10.1103/PhysRevLett.92.181301.

[26] J. N. Bahcall and M. H. Pinsonneault, "What do we (not) know theoretically about solar neutrino fluxes?" *Physical Review Letters*, vol. 92, no. 12, 2004, ISSN: 1079-7114. DOI: 10.1103/physrevlett.92.121301. [Online]. Available: http://dx.doi.org/10.1103/PhysRevLett.92.121301.

[27] T. K. Gaisser and M. Honda, "Flux of atmospheric neutrinos," *Annual Review of Nuclear and Particle Science*, vol. 52, no. 1, pp. 153–199, 2002, ISSN: 1545-4134. DOI: 10.1146/annurev.nucl.52.050102.090645.

[28] K. S. Hirata *et al.*, "Experimental Study of the Atmospheric Neutrino Flux," *Phys. Lett. B*, vol. 205, J. Tran Thanh Van, Ed., p. 416, 1988. DOI: 10.1016/0370-2693(88)91690-5.

[29] Y. Fukuda, T. Hayakawa, E. Ichihara, *et al.*, "Evidence for oscillation of atmospheric neutrinos," *Phys. Rev. Lett.*, vol. 81, pp. 1562–1567, 8 1998. DOI: 10.1103/PhysRevLett.81.1562.

[30] A. Gando, Y. Gando, K. Ichimura, *et al.*, "Constraints on θ_{13} from a three-flavor oscillation analysis of reactor antineutrinos at kamland," *Phys. Rev. D*, vol. 83, p. 052 002, 5 2011. DOI: 10.1103/PhysRevD.83.052002.

[31] M. H. Ahn *et al.*, "Measurement of Neutrino Oscillation by the K2K Experiment," *Phys. Rev. D*, vol. 74, p. 072 003, 2006. DOI: 10.1103/PhysRevD.74.072003. arXiv: hep-ex/0606032.

[32] D. B. collaboration, F. P. An, W. D. Bai, *et al.*, *Precision measurement of reactor antineutrino oscillation at kilometer-scale baselines by daya bay*, 2022. arXiv: 2211.14988 [hep-ex].

[33] K. Zuber, *Neutrino Physics (3rd ed.)* CRC Press, 2020.

[34] S. Abe, S. Asami, M. Eizuka, *et al.*, "Search for the majorana nature of neutrinos in the inverted mass ordering region with kamland-zen," *Physical Review Letters*, vol. 130, no. 5, 2023, ISSN: 1079-7114. DOI: 10.1103/physrevlett.130.051801. [Online]. Available: http://dx.doi.org/10.1103/PhysRevLett.130.051801.

[35] M. Agostini, G. Araujo, A. Bakalyarov, *et al.*, "Final results of gerda on the search for neutrinoless double-β decay," *Physical Review Letters*, vol. 125, no. 25, 2020, ISSN: 1079-7114. DOI: 10.1103/physrevlett.125.252502. [Online]. Available: http://dx.doi.org/10.1103/PhysRevLett.125.252502.

[36] G. Anton, I. Badhrees, P. Barbeau, *et al.*, "Search for neutrinoless double-β decay with the complete exo-200 dataset," *Physical Review Letters*, vol. 123, no. 16, 2019, ISSN: 1079-7114. DOI: 10.1103/physrevlett.123.161802. [Online]. Available: http://dx.doi.org/10.1103/PhysRevLett.123.161802.

[37] S. Bilenky, J. Hošek, and S. Petcov, "On the oscillations of neutrinos with dirac and majorana masses," *Physics Letters B*, vol. 94, no. 4, pp. 495–498, 1980, ISSN: 0370-2693. DOI: https://doi.org/10.1016/0370-2693(80)90927-2. [Online]. Available: https://www.sciencedirect.com/science/article/pii/0370269380909272.

[38] P. Langacker, S. Petcov, G. Steigman, and S. Toshev, "Implications of the mikheyev-smirnov-wolfenstein (msw) mechanism of amplification of neutrino oscillations in matter," *Nuclear Physics B*, vol. 282, pp. 589–609, 1987, ISSN: 0550-3213. DOI: https://doi.org/10.1016/0550-3213(87)90699-7.

[39] I. Esteban, M. C. Gonzalez-Garcia, M. Maltoni, T. Schwetz, and A. Zhou, "The fate of hints: updated global analysis of three-flavor neutrino oscillations," *JHEP*, vol. 09, p. 178, 2020. DOI: 10.1007/JHEP09(2020)178. arXiv: 2007.14792 [hep-ph].

[40] *Nufit 5.3*, Available online at: http://www.nu-fit.org; accessed on 12/03/2024., 2024.

[41] *All things neutrino*, Fermi National Accelerator Laboratory website (2023). Online available at: https://neutrinos.fnal.gov/mysteries/mass-ordering/#moreinfo; accessed on 02/02/2024.

[42] T. Ferbel, *Techniques and Concepts of High Energy Physics X* (Nato Science Series C). Springer Dordrecht, 1999, pp. 263–267.

[43] C. Athanassopoulos, L. B. Auerbach, D. A. Bauer, *et al.*, "Candidate events in a search for $\overline{\nu}_\mu \to \overline{\nu}_e$ oscillations," *Phys. Rev. Lett.*, vol. 75, pp. 2650–2653, 14 1995. DOI: 10.1103/PhysRevLett.75.2650.

[44] B. Armbruster, I. M. Blair, B. A. Bodmann, *et al.*, "Upper limits for neutrino oscillations $\overline{\nu}_\mu \to \overline{\nu}_e$ from muon decay at rest," *Phys. Rev. D*, vol. 65, p. 112 001, 11 2002. DOI: 10.1103/PhysRevD.65.112001.

[45] A. Aguilar, L. B. Auerbach, R. L. Burman, *et al.*, "Evidence for neutrino oscillations from the observation of $\overline{\nu}_e$ appearance in a $\overline{\nu}_\mu$ beam," *Phys. Rev. D*, vol. 64, p. 112 007, 11 2001. DOI: 10.1103/PhysRevD.64.112007.

[46] A. A. Aguilar-Arevalo, C. E. Anderson, A. O. Bazarko, *et al.*, "Neutrino flux prediction at miniboone," *Phys. Rev. D*, vol. 79, p. 072 002, 7 2009. DOI: 10.1103/PhysRevD.79.072002.

[47] A. A. Aguilar-Arevalo *et al.*, "The MiniBooNE Detector," *Nucl. Instrum. Meth. A*, vol. 599, pp. 28–46, 2009. DOI: 10.1016/j.nima.2008.10.028. arXiv: 0806.4201 [hep-ex].

[48] A. A. Aguilar-Arevalo, C. E. Anderson, S. J. Brice, *et al.*, "Measurement of the neutrino component of an antineutrino beam observed by a nonmagnetized detector," *Phys. Rev. D*, vol. 84, p. 072 005, 7 2011. DOI: 10.1103/PhysRevD.84.072005.

[49] A. A. Aguilar-Arevalo, A. O. Bazarko, S. J. Brice, *et al.*, "Search for electron neutrino appearance at the $\Delta m^2 \sim 1$ eV^2 scale," *Phys. Rev. Lett.*, vol. 98, p. 231 801, 23 2007. DOI: 10.1103/PhysRevLett.98.231801.

[50] A. A. Aguilar-Arevalo *et al.*, "Unexplained Excess of Electron-Like Events From a 1-GeV Neutrino Beam," *Phys. Rev. Lett.*, vol. 102, p. 101 802, 2009. DOI: 10.1103/PhysRevLett.102.101802. arXiv: 0812.2243 [hep-ex].

[51] A. A. Aguilar-Arevalo, B. C. Brown, J. M. Conrad, *et al.*, "Updated miniboone neutrino oscillation results with increased data and new background studies," *Phys. Rev. D*, vol. 103, p. 052 002, 5 2021. DOI: 10.1103/PhysRevD.103.052002.

[52] *Imaging atmospheric cherenkov technique*, Sera Markoff blog. Online available at: https://www.seramarkoff.com/2018/10/imaging-atmospheric-cherenkov-technique/; accessed on 02/02/2024.

[53] A. A. Aguilar-Arevalo, B. C. Brown, L. Bugel, *et al.*, "Significant excess of electron-like events in the miniboone short-baseline neutrino experiment," *Phys. Rev. Lett.*, vol. 121, p. 221 801, 22 2018. DOI: 10.1103/PhysRevLett.121.221801.

[54] T. Katori and J. M. Conrad, "Beyond standard model searches in the miniboone experiment," *Advances in High Energy Physics*, vol. 2015, no. 1, p. 362 971, 2015. DOI: https://doi.org/10.1155/2015/362971.

[55] A. A. Aguilar-Arevalo, C. E. Anderson, S. J. Brice, *et al.*, "Event excess in the miniboone search for $\overline{\nu}_\mu \to \overline{\nu}_e$ oscillations," *Phys. Rev. Lett.*, vol. 105, p. 181 801, 18 2010. DOI: 10.1103/PhysRevLett.105.181801.

[56] A. A. Aguilar-Arevalo *et al.*, "A Combined $\nu_\mu \to \nu_e$ and $\bar{\nu}_\mu \to \bar{\nu}_e$ Oscillation Analysis of the MiniBooNE Excesses," 2012. arXiv: 1207.4809 [hep-ex].

[57] D. Sluse, *Programming techniques, numerical methods and machine learning*, Master in Space sciences course dispensed at the University of Liège. The Github repository of this course is accessible online at https://github.com/SPAT0002-1/Ongoing., 2021.

[58] T. Kajita, "Atomspheric neutrinos and discovery of neutrino oscillations," *Proc. Japan Acad. B*, vol. 86, pp. 303–321, 2010. DOI: 10.2183/pjab.86.303.

[59] *Resolution b2 on the re-definition of the astronomical unit of length.* Online available at: https://syrte.obspm.fr/IAU_resolutions/Res_IAU2012_B2.pdf; accessed on 15/07/2024., 2012.

[60] A. Prša, P. Harmanec, G. Torres, *et al.*, "Nominal values for selected solar and planetary quantities: Iau 2015 resolution b3," *The Astronomical Journal*, vol. 152, no. 2, p. 41, 2016, ISSN: 1538-3881. DOI: 10.3847/0004-6256/152/2/41.

[61] J. N. Abdurashitov, V. N. Gavrin, V. V. Gorbachev, *et al.*, "Measurement of the solar neutrino capture rate with gallium metal. iii. results for the 2002–2007 data-taking period," *Physical Review C*, vol. 80, no. 1, 2009, ISSN: 1089-490X. DOI: 10.1103/physrevc.80.015807.

[62] F. Kaether, W. Hampel, G. Heusser, J. Kiko, and T. Kirsten, "Reanalysis of the gallex solar neutrino flux and source experiments," *Physics Letters B*, vol. 685, no. 1, pp. 47–54, 2010, ISSN: 0370-2693. DOI: 10.1016/j.physletb.2010.01.030.

[63] K. e. a. Abe, "Solar neutrino measurements using the full data period of super-kamiokande-iv," *Physical Review D*, vol. 109, no. 9, 2024, ISSN: 2470-0029. DOI: 10.1103/physrevd.109.092001.

[64] J. Nocedal and S. J. Wright, *Numerical Optimization*. New York, NY, USA: Springer, 1999.

[65] J. A. Nelder and R. Mead, "A simplex method for function minimization," *Comput. J.*, vol. 7, pp. 308–313, 1965.

[66] S. G. Nash, "Newton-type minimization via the lanczos method," *SIAM Journal on Numerical Analysis*, vol. 21, no. 4, pp. 770–788, 1984, ISSN: 00361429. [Online]. Available: http://www.jstor.org/stable/2157008.

[67] J. N. Abdurashitov, V. N. Gavrin, S. V. Girin, *et al.*, "Measurement of the response of a ga solar neutrino experiment to neutrinos from an 37ar source," *Physical Review C*, vol. 73, no. 4, 2006, ISSN: 1089-490X. DOI: 10.1103/physrevc.73.045805.

[68] C. Giunti and M. Laveder, "Statistical significance of the gallium anomaly," *Phys. Rev. C*, vol. 83, p. 065 504, 6 2011. DOI: 10.1103/PhysRevC.83.065504.

[69] G. Mention, M. Fechner, T. Lasserre, *et al.*, "Reactor antineutrino anomaly," *Physical Review D*, vol. 83, no. 7, 2011, ISSN: 1550-2368. DOI: 10.1103/physrevd.83.073006.

[70] M. Soderberg, F. Sanchez, M. Sorel, and L. Alvarez-Ruso, "Microboone: A new liquid argon time projection chamber experiment," in *AIP Conference Proceedings*, AIP, 2009. DOI: 10.1063/1.3274193.

[71] P. Abratenko, R. An, J. Anthony, *et al.*, "Search for neutrino-induced neutral-current Δ radiative decay in microboone and a first test of the miniboone low energy excess under a single-photon hypothesis," *Physical Review Letters*, vol. 128, no. 11, 2022, ISSN: 1079-7114. DOI: 10.1103/physrevlett.128.111801.

[72] M. Drewes, "The phenomenology of right handed neutrinos," *International Journal of Modern Physics E*, vol. 22, no. 08, 2013, ISSN: 1793-6608. [Online]. Available: https://arxiv.org/abs/1303.6912.

[73] B. Dasgupta and J. Kopp, "Sterile neutrinos," *Physics Reports*, vol. 928, pp. 1–63, 2021, ISSN: 0370-1573. DOI: 10.1016/j.physrep.2021.06.002. [Online]. Available: http://dx.doi.org/10.1016/j.physrep.2021.06.002.

[74] K. Abe, Y. Haga, Y. Hayato, *et al.*, "Limits on sterile neutrino mixing using atmospheric neutrinos in super-kamiokande," *Physical Review D*, vol. 91, no. 5, 2015, ISSN: 1550-2368. DOI: 10.1103/physrevd.91.052019.

[75] J. M. Conrad, C. M. Ignarra, G. Karagiorgi, M. H. Shaevitz, and J. Spitz, *Sterile neutrino fits to short baseline neutrino oscillation measurements*, 2012. arXiv: 1207.4765 [hep-ex].

[76] A. Aguilar-Arevalo, B. Brown, J. Conrad, *et al.*, "Miniboone and microboone combined fit to a $3 + 1$ sterile neutrino scenario," *Physical Review Letters*, vol. 129, no. 20, 2022, ISSN: 1079-7114. DOI: 10.1103/physrevlett.129.201801.

[77] E. D. Valentino, S. Gariazzo, and O. Mena, *Neutrinos in cosmology*, 2024. arXiv: 2404.19322 [astro-ph.CO]. [Online]. Available: https://arxiv.org/abs/2404.19322.

[78] R. Acciarri, C. Adams, R. An, *et al.*, *A proposal for a three detector short-baseline neutrino oscillation program in the fermilab booster neutrino beam*, 2015. arXiv: 1503.01520 [physics.ins-det].

[79] M. Bonesini, *The short baseline neutrino program at fermilab*, 2022. arXiv: 2203.05814 [hep-ex].

[80] D. Jena, "The DUNE Experiment," *PoS*, vol. HQL2023, p. 023, 2024. DOI: 10.22323/1.462.0023.

[81] S. Ajimura, M. Botran, J. Choi, *et al.*, "The jsns^2 detector," *Nuclear Instruments and Methods in Physics Research Section A: Accelerators, Spectrometers, Detectors and Associated Equipment*, vol. 1014, p. 165 742, 2021, ISSN: 0168-9002. DOI: 10.1016/j.nima.2021.165742. [Online]. Available: http://dx.doi.org/10.1016/j.nima.2021.165742.

[82] D. H. Lee, S. Ajimura, M. K. Cheoun, *et al.*, "Study on the accidental background of the jsns^2 experiment," *The European Physical Journal C*, vol. 84, no. 4, 2024, ISSN: 1434-6052. DOI: 10.1140/epjc/s10052-024-12778-7.

[83] H.-K. Proto-Collaboration, : K. Abe, *et al.*, *Hyper-kamiokande design report*, 2018. arXiv: 1805.04163 [physics.ins-det]. [Online]. Available: https://arxiv.org/abs/1805.04163.